considered. In particular, our dose setting for the database was based on preliminary experiments of repeated dosing for 7 days with the proviso that all animals are to survive for 28 days. This sometimes brings about a situation that the dose level is too low for certain phenotypes. This point is particularly problematic when biomarker gene lists are to be extracted based on the actually observed phenotype. Of these 6 drugs, we could judge CMP, PMZ and TMX as positive by PCA using the present marker genes, whereas CPZ, GMC and PH were weakly positive or almost negative. These observations could be due to a feature of the marker genes: a considerable part of them actually reflects the occurring pathological changes, namely, they work as diagnostic markers. The fact that some of the drugs could be judged as positive suggested that their diagnosis from marker genes was more sensitive than pathological examination.

GMC has been reported to cause PLsis in kidney tissue and this is associated with renal tubular toxicity (Kaloyanides and Pastoriza-Munoz, 1980; Laurent et al., 1990). This might be attributed to its negative judgment for PLsis in liver since potential biochemical/pathological changes would mainly occur in kidney. It is of interest to investigate the gene expression changes in kidney, but another set of genes would be necessary to make a precise diagnosis for PLsis in kidney.

PH was selected as a PLsis-positive drug but appeared to be negative or a very weak positive in the present study using rats. This might be due to the species difference in the drug metabolism since the risk of PH-induced liver injury is higher in individuals with the P450IID6 poor-metabolizer phenotype (Morgan et al., 1984, Pessayre and Larrey, 1988).

Some compounds show morphological changes similar to PLsis. In our database, there are 8 such compounds, i.e., CCL4, CMA, TC, MFM, HYZ, DIL, BEA, and ETH. Of these, CCL4 (Weber et al., 2003), TC (Fréneaux et al., 1988), BEA (Thiele-

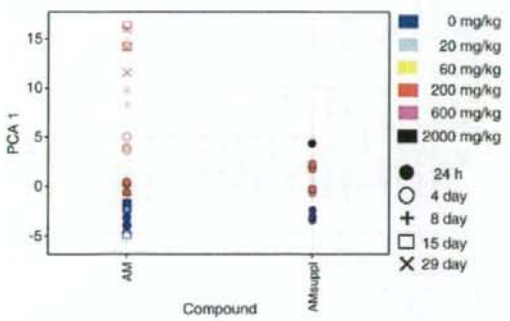

Fig. 6. Principal component analysis of gene expression profiles of amiodarone. Results are expressed as a one dimensional figure with PC1 (contribution rate: 34.8%). Each individual rat is depicted by a symbol with a different color and shape as shown on the right panel. On the left, the data of 24 h after a single treatment (filled symbols) are added to the data for repeated treatment (open or line symbols) shown in the previous figures. Note that the PC1 value of a single dose is low even at the highest dose, 200 mg/kg (red filled circle) compared with the repeated dose (red open or line symbols). On the left, a supplemental higher dose experiment was performed. Note that the higher dose (600 mg/kg, magenta; 2000 mg/kg, black) showed a dose-dependent increase in PC1 reaching to a value of 200 mg/kg at 4 days.

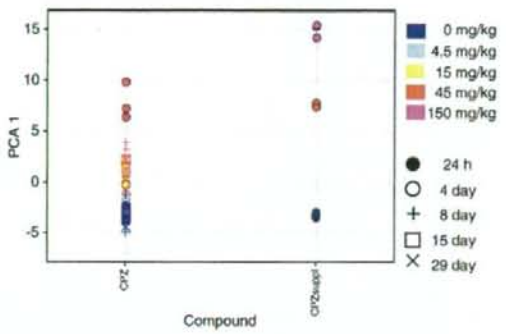

Fig. 7. Principal component analysis of gene expression profiles of chlorpromazine. Results are expressed as a one dimensional figure with PC1 (contribution rate: 34.8%). Each individual rat is depicted by a symbol with a different color and shape as shown on the right panel. On the left, the data of 24 h after a single treatment (filled symbols) are added to the data for repeated treatment (open or line symbols) shown in the previous figures. In contrast to the results in Fig. 6, the single dose of 45 mg/kg (red filled circle) gave higher PC1 values compared with samples of repeated dosing. On the left, a supplemental higher dose (150 mg/kg) experiment was performed in addition to 45 mg/kg. Note that the higher dose (magenta) showed even higher PC1 values.

mann et al., 1999), and ETH (Kuntz et al., 1968, Inouye et al., 1973) are reported to show morphology associated with a change in the lipid storage, i.e., lipidosis or steatosis. CMA is known to cause hepatic necrosis (Lake, 1984) and MFM induces a deposition of glycogen. These drugs, which do not induce PLsis, could be separated from the clusters of PLsis-inducing ones by PCA using the extracted genes. As for HYZ (Hruban et al., 1972), classified as PLsis-positive by PCA in this study, there is a recent report that it actually induced PLsis (Pelletier et al., 2007). The only exception was the case of DIL, which showed vacuolation in hepatocytes and was not considered as PLsis, but was classified as positive by PCA. Reviewing the PCA (Fig. 5) however, it is noticeable that the time-dependent changes in the PC1 value are exceptionally different from other drugs such that the value transiently increases with the peak at 4 days, then decreases with time and returns to negative at the 15th day. It is necessary to elucidate the mechanism of the unique change observed in DIL, but it appears that this drug is to be judged as pseudo-positive by the present criteria.

One important question is whether the toxicogenomics approach enables not only diagnosis but also prognosis of PLsis. The results shown in Figs. 6 and 7 provide a clue. In general, it appears to be difficult to predict the potential of PLsis occurring 14 days or later with repeated administration with the data for single dosing, but it could be possible when a high enough dose is applied in some cases. We are presently in a preliminary stage, but we hope to establish a really useful marker gene set in a future study with a strategic protocol, which can predict PLsis in liver by single dosing within 24 h. In the present study, we exclusively worked on liver where enough gene expression data are stored in our database. As PLsis occurs in organs other than liver, it is of interest to apply the present strategy to other organs such as kidney whose transcriptome data are now accumulating in our database.

There remain many problems to be solved in the present system, such as the improvement of accuracy and sensitivity, the elucidation of the functions of the genes in the list (especially in the pathological mechanism of PLsis), the breakthrough species difference, and so on. However, the presently identified 78 probe sets from gene expression data stored in TG-GATEs have provided a powerful starting tool.

Acknowledgment

This work was supported in part by the grants from Ministry of Health, Labour and Welfare of Japan, H14-001-Toxico.

References

Casartelli, A., Bonato, M., Cristofori, P., Crivellente, F., Dal Negro, G., Masotto, I., Mutinelli, C., Valko, K., Bonfante, V., 2003. A cell-based approach for the early assessment of the phospholipidogenic potential in pharmaceutical research and drug development. Cell Biol. Toxicol. 19, 161–176.

Dennis Jr., G., Sherman, B.T., Hosack, D.A., Yang, J., Gao, W., Lane, H.C., Lempicki, R.A., 2003. DAVID: database for annotation, visualization, and integrated discovery. Genome Biol. 4, P3.

Drenckhahn, D., Kleine, L., Lullmann-Rauch, R., 1976. Lysosomal alterations in cultured macrophages exposed to anorexigenic and psychotropic drugs. Lab. Invest. 35, 116–123.

Drew, R., Siddik, Z.H., Mimnaugh, E.G., Gram, T.E., 1981. Species and dose differences in the accumulation of imipramine by mammalian lungs. Drug Metab. Dispos. 9, 322–326.

Fréneaux, E., Labbe, G., Letteron, P., The Le Dinhi, Degott, C., Genève, J., Larrey, D., Pessayre, D., 1988. Inhibition of the mitochondrial oxidation of fatty acids by tetracycline in mice and in man: possible role in microvesicular steatosis induced by this antibiotic. Hepatology 8, 1056–1062.

Halliwell, W.H., 1997. Cationic amphiphilic drug-induced phospholipidosis. Toxicol. Pathol. 25, 53–60.

Hansson, A.L., Xia, Z., Berglund, M.C., Bergstrand, A., Depierre, J.W., Nässberger, L., 1997. Reduced cell survival and morphological alterations induced by three tricyclic antidepressants in human peripheral monocytes and lymphocytes and in cell lines derived from these cell types. Toxicol. In Vitro 11, 21–31.

Honegger, U.E., Zuehlke, R.D., Scuntaro, L., Schaefer, M.H., Toplak, H., Wiesmann, U.N., 1993. Cellular accumulation of amiodarone and desethylamiodarone in cultured human cells. Consequences of drug accumulation on cellular lipid metabolism and plasma membrane properties of chronically exposed cells. Biochem. Pharmacol. 45, 349–356.

Hruban, Z., Slesers, A., Hopkins, E., 1972. Drug-induced and naturally occurring myeloid bodies. Lab. Invest. 27, 62–70.

Inouye, B., Yoshimura, N., Wachi, T., 1973. Experimental studies on the mechanism of fatty liver formation induced by ethionamide. V. Liver and serum total cholesterol in ethionamide-administered rats. Kekkaku 48, 71–74.

Joshi, U.M., Rao, P., Kodavanti, S., Lockard, V.G., Mehendale, H.M., 1989. Fluorescence studies on binding of amphiphilic drugs to isolated lamellar bodies: relevance to phospholipidosis. Biochim. Biophys. Acta 1004, 309–320.

Kacew, S., 1987. Cationic amphiphilic drug-induced renal cortical lysosomal phospholipidosis: an in vivo comparative study with gentamicin and chlorphentermine. Toxicol. Appl. Pharmacol. 91, 469–746.

Kaloyanides, G.J., Pastoriza-Munoz, E., 1980. Aminoglycoside nephrotoxicity. Kidney Int. 18, 571–582.

Kasahara, T., Tomita, K., Murano, H., Harada, T., Tsubakimoto, K., Ogihara, T., Ohnishi, S., Kakinuma, C., 2006. Establishment of an in vitro high-throughput screening assay for detecting phospholipidosis-inducing potential. Toxicol. Sci. 90, 133–141.

Kodavanti, U.P., Lockard, V.G., Mehendale, H.M., 1990. In vivo toxicity and pulmonary effects of promazine and chlorpromazine in rats. J. Biochem. Toxicol. 5, 245–251.

Kuntz, E., Lichr, H., Pfingst, W., 1968. Toxic liver damage due to ethionamide. Ger. Med. Mon. 13, 599–602.

Lake, B.G., 1984. Investigations into the mechanism of coumarin-induced hepatotoxicity in the rat. Arch. Toxicol. Suppl. 7, 16–29.

Laurent, G., Kishore, B.K., Tulkens, P.M., 1990. Aminoglycoside-induced renal phospholipidosis and nephrotoxicity. Biochem. Pharmacol. 40, 2383–2392.

Morgan, M.Y., Reshef, R., Shah, R.R., Oates, N.S., Smith, R.L., Sherlock, S., 1984. Impaired oxidation of debrisoquine in patients with perhexiline liver injury. Gut 25, 1057–1064.

Nioi, P., Perry, B.K., Wang, E.J., Gu, Y.Z., Snyder, R.D., 2007. In vitro detection of drug-induced phospholipidosis using gene expression and fluorescent phospholipid based methodologies. Toxicol. Sci. 99, 162–173.

Pelletier, D.J., Gehlhaar, D., Tilloy-Ellul, A., Johnson, T.O., Greene, N., 2007. Evaluation of a published in silico model and construction of a novel bayesian model for predicting phospholipidosis inducing potential. J. Chem. Inf. Model 47, 1196–1205.

Pessayre, D., Bichara, M., Degott, C., Potet, F., Benhamou, J.P., Feldmann, G., 1979. Perhexiline maleate-induced cirrhosis. Gastroenterol. 76, 170–177.

Pessayre, D., Larrey, D., 1988. Acute and chronic drug-induced hepatitis. Baillieres Clin. Gastroenterol. 2, 385–422.

Reasor, M.J., Kacew, S., 2001. Drug-induced phospholipidosis: are there functional consequences? Exp. Biol. Med. 226, 825–830.

Reasor, M.J., Hastings, K.L., Ulrich, R.G., 2006. Drug-induced phospholipidosis: issues and future directions. Expert Opin. Drug Saf. 5, 567–583.

Sawada, H., Takami, K., Asahi, S., 2005. A toxicogenomic approach to drug-induced phospholipidosis: analysis of its induction mechanism and establishment of a novel in vitro screening system. Toxicol. Sci. 83, 282–292.

Sawada, H., Taniguchi, K., Takami, K., 2006. Improved toxicogenomic screening for drug-induced phospholipidosis using a multiplexed quantitative gene expression ArrayPlate assay. Toxicol. In Vitro 20, 1506–1513.

Takashima, K., Mizukawa, Y., Morishita, K., Okuyama, M., Kasahara, T., Toritsuka, N., Miyagishima, T., Nagao, T., Urushidani, T., 2006. Effect of the difference in vehicles on gene expression in the rat liver-analysis of the control data in the Toxicogenomics Project Database. Life Sci. 78, 2787–2796.

Thiclemann, L.E., Bosco, C., Rodrigo, R., Orellana, M., Videla, L.A., 1999. Effects of bromoethylamine on antioxidant capacity, lipid peroxidation, and morphological characteristics of rat liver. J. Biochem. Mol. Toxicol. 13, 47–52.

Tomizawa, K., Sugano, K., Yamada, H., Horii, I., 2006. Physicochemical and cell-based approach for early screening of phospholipidosis-inducing potential. J. Toxicol. Sci. 31, 315–324.

Urushidani, T., Nagao, T., 2005. Toxicogenomics: the Japanese initiative. In: Borlak, J. (Ed.), Handbook of Toxicogenomics—Strategies and Applications. Wiley-VCH, pp. 623–631.

Weber, L.W., Boll, M., Stampfl, A., 2003. Hepatotoxicity and mechanism of action of haloalkanes: carbon tetrachloride as a toxicological model. Crit. Rev. Toxicol. 33, 105–136.

Whitehouse, L.W., Menzies, A., Mueller, R., Pontefract, R., 1994. Ketoconazole-induced hepatic phospholipidosis in the mouse and its association with de-*N*-acetyl ketoconazole. Toxicology 94, 81–95.

Xia, Z., Ying, G., Hansson, A.L., Karlsson, H., Xie, Y., Bergstrand, A., DePierre, J.W., Nassberger, L., 2000. Antidepressant-induced lipidosis with special reference to tricyclic compounds. Prog. Neurobiol. 60, 501–512.

Human & Experimental Toxicology (2008) 27: 23–35
www.het.sagepub.com

Species-specific differences in coumarin-induced hepatotoxicity as an example toxicogenomics-based approach to assessing risk of toxicity to humans

T Uehara[1], N Kiyosawa[1], T Shimizu[1], K Omura[1], M Hirode[1], T Imazawa[1], Y Mizukawa[2], A Ono[1], T Miyagishima[1], T Nagao[3] and T Urushidani[1,2]

[1]Toxicogenomics Project, National Institute of Biomedical Innovation, Ibaraki, Osaka, Japan; [2]Department of Pathophysiology, Faculty of Pharmaceutical Sciences, Doshisha Women's College of Liberal Arts, Kyotanabe, Kyoto, Japan; and [3]National Institute of Health Sciences, Setagaya-ku, Tokyo, Japan

One expected result from toxicogenomics technology is to overcome the barrier because of species-specific differences in prediction of clinical toxicity using animals. The present study serves as a model case to test if the well-known species-specific difference in the toxicity of coumarin could be elucidated using comprehensive gene expression data from rat in-vivo, rat in-vitro, and human in-vitro systems. Coumarin 150 mg/kg produced obvious pathological changes in the liver of rats after repeated administration for 7 days or more. Moreover, 24 h after a single dose, we observed minor and transient morphological changes, suggesting that some early events leading to hepatic injury occur soon after coumarin is administered to rats. Comprehensive gene expression changes were analyzed using an Affymetrix GeneChip® approach, and differentially expressed probe sets were statistically extracted. The changes in expression of the selected probe sets were further examined in primary cultured rat hepatocytes exposed to coumarin, and differentially expressed probe sets common to the in-vivo and in-vitro datasets were selected for further study. These contained many genes related to glutathione metabolism and the oxidative stress response. To incorporate human data, human hepatocyte cultured cells were exposed to coumarin and changes in expression of the bridging gene set were examined. In total, we identified 14 up-regulated and 11 down-regulated probe sets representing rat–human bridging genes. The overall responsiveness of these genes to coumarin was much higher in rats than humans, consistent with the reported species difference in coumarin toxicity. Next, we examined changes in expression of the rat–human bridging genes in cultured rat and human hepatocytes treated with another hepatotoxicant, diclofenac sodium, for which hepatotoxicity does not differ between the species. Both rat and human hepatocytes responded to the marker genes to the same extent when the same concentrations of diclofenac sodium were exposed. We conclude that toxicogenomics-based approaches show promise for overcoming species-specific differences that create a bottleneck in analysis of the toxicity of potential therapeutic treatments.

Key words: coumarin; hepatocyte; hepatotoxicity; human; liver; rat; toxicogenomics

Introduction

The Toxicogenomics Project (TGP) is a 5-year collaborative project of the National Institute of Health Sciences, the National Institute of Biomedical Innovation, and 15 pharmaceutical companies in Japan that began in 2002.[1] The aim was to construct a large-scale toxicology database of transcriptomes useful to predict the toxicity of new chemical entities in early stages of drug development. About 150 chemicals, primarily medicinal compounds, were selected and gene expression in the rat liver (also kidney in some cases) or rat and human hepatocytes was comprehensively analyzed by using the Affymetrix GeneChip®.[2] In 2007, the project was completed and the whole system, consisting of a database, an analysis system, and a prediction system, was completed and named TG-GATEs (for Genomics Assisted Toxicity Evaluation System developed by Toxicogenomics Project in Japan).

Correspondence to: Tetsuro Urushidani, Department of Pathophysiology, Faculty of Pharmaceutical Sciences, Doshisha Women's College of Liberal Arts, Kodo, Kyotanabe, Kyoto 610-0395, Japan. Email: turushid@dwc.doshisha.ac.jp

10.1177/0960327107087910

The main purpose of creating the system was to facilitate analysis of the mechanisms of toxicity and prediction of chronic toxicity from acute data in preclinical studies, and the consensus response to the project is that toxicogenomics-based technologies provide a useful tool. However, the final goal of a preclinical study should be prediction of clinical toxicity based on animal data. Toward this end, overcoming species-specific differences has proved to be the most difficult problem. We expect that elucidation of mechanisms of toxicity using toxicogenomics-based tools should lead to an improved ability to use animal data to make reasonable predictions of toxicity in humans.[3] However, there have been few reports of species-specific differences in the toxicological response at the level of changes in gene expression.[4]

We obtained gene expression data from rat primary hepatocytes as well as human frozen hepatocytes (in addition to rat in-vivo liver) to build an informational bridge between the two species. In the present study, we analyzed the effects of coumarin, a representative hepatotoxicant with a known species-specific difference in toxicity, as a model case for determining if species-specific differences in hepatotoxicity can be accurately predicted using a toxicogenomics-based approach.

Materials and methods

Chemicals

Coumarin and diclofenac sodium (DFNa) were obtained from Tokyo Chemical Industry (Tokyo, Japan).

Animal Treatment

All experimental protocols using animals were reviewed and approved by the Ethics Review Committee for Animal Experimentation of the National Institute of Health Sciences. The experimental protocols using human hepatocytes were reviewed and approved by both the Ethics Review Committees for Experimentation on Human Subjects of the National Institute of Health Sciences and of the National Institute of Biomedical Innovation.

Five-week-old male Sprague-Dawley rats were obtained from Charles River Japan Inc. (Kanagawa, Japan). After a 7-day quarantine and acclimatization period, 6-week-old animals were assigned to dosage groups (five rats per group) using a computerized stratified random grouping method based on individual body weight. The animals were individually housed in stainless-steel cages in an animal room that was lighted for 12 h (7:00–19:00) daily, ventilated with an air-exchange rate of 15 times per hour and maintained at 21–25 °C with a relative humidity of 40–70%. Each animal was allowed free access to water and pellet diet (CRF-1, sterilized by radiation; Oriental Yeast Co., Ltd., Tokyo, Japan).

Either vehicle (corn oil), or 15, 50, or 150-mg/kg coumarin was administered orally to rats once daily on day 1, 3, 7, 14, and 28, and the animals were euthanized 24 h after the last dosing by exsanguination from the abdominal aorta under ether anesthesia. Liver samples were obtained from the left lateral lobe of the liver of each animal immediately after sacrifice. For light microscopy, liver samples were fixed in 10% neutral-buffered formalin, dehydrated in alcohol, and embedded in paraffin. Paraffin sections were prepared and stained using standard methods for hematoxylin and eosin staining. Histopathological findings were graded into four categories: very slight, slight, moderate, and severe. For electron microscopy, a piece of tissue from the liver was fixed in 2.5% glutaraldehyde solution. Ultra-thin sections, stained with Mayer's hematoxylin and lead citrate after standard tissue processing, were observed under a Hitachi electron microscope (H-7650; Hitachi High-Technologies Corporation Tokyo, Japan).

Hepatocyte treatment

Hepatocytes were isolated from 6-week-old male Sprague-Dawley rats under sodium pentobarbital (120 mg/kg, i.p.) and anesthetized using a modified two-step collagenase perfusion method. The liver was perfused via the portal vein for 10 min with divalent, cation-free, EGTA (ethylene glycol-bis[β-aminoethyl ether]-N,N,N',N'-tetraacetic acid) (0.5 mM)-supplemented HEPES (4-(2-hydroxyethyl)-1-piperazineethanesulfonic acid)-buffered Hank's balanced salt solution followed by a 10-min perfusion with HEPES (10 mM)-buffered normal Hank's balanced salt solution containing soybean trypsin inhibitor (0.05 g/L, T-2011; Sigma Aldrich, St Louis, Missouri, USA) and collagenase (0.5 g/L, 034-10533; Wako Pure Chemical Industries, Osaka, Japan) at a flow rate of 10–30 mL/min. The isolated cells were washed three times and centrifugated at 50 × *g* for 1 min to obtain a parenchymal cell-enriched pellet. Hepatocytes were not used when their viability was <70% (as assessed by trypan blue exclusion). Cell samples that passed the threshold for viability were seeded into collagen-coated six-well plates (BD BioCoat™ Collagen I Cellware; BD Bioscience, Bedford, Massachusetts, USA) at a density of 1×10^6 cells/well in 2 mL HMC Bulletkit medium (Cambrex,

Walkersville, Maryland, USA) supplemented with 10% fetal bovine serum.

For human hepatocytes (Tissue Transformation Technologies Inc., presently BD Biosciences, San Jose, California, USA), the frozen cells were thawed, washed twice with medium (L15 medium supplemented with penicillin, streptomycin, and 10% fetal bovine serum), and then seeded as described for rat hepatocytes except that the cell density was 1.2×10^6 cells/well.

Following an attachment period of 3 h, the medium was replaced and kept overnight before exposure to the drug at 37 °C in an atmosphere of 5% CO_2. The test compounds were added to the medium directly or as a 1000× stock solution in dimethylsulfoxide (DMSO). After 2, 8, or 24-h exposure, cells were dissolved with RLT buffer (Qiagen, Valencia, California, USA) and collected for expression profiling. GeneChip analysis was performed in duplicate for each concentration.

Cell viability was assessed by monitoring leakage of lactate dehydrogenase (LDH). To do this, both the culture medium and the cell lysate (lysis with 0.1% Triton X-100) were analyzed using an automatic biochemical analyzer (TBA-200FR; Toshiba, Tokyo, Japan) and the rate of survival relative to a control was calculated as follows: $LDH_{cell}/(LDH_{cell} + LDH_{medium})$.

The appropriate concentrations of test drugs were determined in a preliminary experiment. For our general protocol, the highest concentration was set to 10–20% of the lethal concentration as estimated by LDH leakage over 24 h. When the cells could tolerate as much as 10 mM or the level equal to the solubility limit of the compound in DMSO (allowed to add up to 0.1% in the final concentration), the highest concentration was set to either value. Exposures were performed at two different concentrations, 1/5 and 1/25 of the highest concentration. In case of coumarin, no LDH leakage was observed for either rat or human hepatocytes after treatment with concentrations of up to 300 μM, which was the solubility limit. Thus, concentrations of 12, 60, and 300 μM coumarin were used in subsequent assays. For DFNa, 400 μM was set as the maximum both in rats and humans. Thus, concentrations of 16, 80, and 400 μM DFNa were used in subsequent assays.

GeneChip analysis

For analysis of rat livers, microarray analysis was conducted on three of five samples from each single dose group (24-h post-dose) using GeneChip® RAE 230A probe arrays (Affymetrix, Santa Clara, California, USA). Liver samples were homogenized with buffer RLT supplied with the RNeasy Mini Kit (Qiagen) and total RNA was isolated according to the manufacturer's instructions.

For hepatocytes, GeneChip analysis was performed in duplicate for each concentration using RAE230 2.0 probe arrays for rat hepatocytes and U133 Plus 2.0 arrays for human hepatocytes (Affymetrix). Cells were dissolved with RLT buffer and collected for expression profiling. Different versions were used for the in-vitro versus the in-vivo study because RAE230 2.0 was released after the in-vivo experiments were completed. The procedure was conducted basically as described in the manufacturer's instructions using Superscript Choice System (Invitrogen, Carlsbad, California, USA) and T7-(dT)24-oligonucleotide primer (Affymetrix) for cDNA synthesis, cDNA Cleanup Module (Affymetrix) for purification, and BioArray High yield RNA Transcript Labeling Kit (Enzo Diagnostics, Farmingdale, New York, USA) for synthesis of biotin-labeled cRNA. Ten micrograms of fragmented cRNA was hybridized to a RAE230A probe array for 18 h at 45 °C at 60 rpm, after which the array was washed and stained with streptavidin–phycoerythrin using Fluidics Station 400 (Affymetrix) and scanned with a Gene Array Scanner (Affymetrix). The digital image files were processed using Affymetrix Microarray Suite version 5.0. Microarray image data were analyzed with GeneChip Operating Software (Affymetrix). All microarray data were scaled by global normalization with the mean signal intensity of all data adjusted to 500.

Gene expression data analysis

To identify genes that are differentially expressed after in-vivo coumarin treatment, the Student's *t*-test was applied with a *P* value cut-off of 0.05 in combination with fold changes of 2.0 or greater and 0.5 or less using Spotfire® DecisionSite for Functional Genomics (Spotfire, Göteborg, Sweden). Probe sets designated as absent by an Affymetrix detection call in any of six samples (three each for control and treated) were excluded from further analysis.

To extract genes that changed in response to coumarin in both the in-vivo and in-vitro sample groups, the changes in expression of the above-mentioned probe sets were examined in rat hepatocytes treated with the high dose (300 μM) of coumarin. Probe sets showing 1.5-fold or greater (up-regulated) and 0.6-fold or less (down-regulated) were selected.

In the next step, the genes in common to the in-vivo and in-vitro rat assays were compared in rat versus human hepatocytes. To do this, we first examined public data on human orthologs of the

rat genes (NetAffx[5]). Upon assignment of orthologs, rat probes sets without human ortholog information were excluded. Because for the redundant probe sets for human samples, a single probe set was selected based on the reliability and dose-dependency of the expression profile. Finally, the probe sets, which were designated as absent by Affymetrix detection, call in seven or more out of eight samples (two each for control and high dose treated in rat and human) were excluded from further analysis.

To facilitate analysis in the large-scale microarray database, we developed two types of one-dimensional score, TGP1 and TGP2, which express the trends in changes in expression of biomarker genes as a whole. The former is based on the signal log ratio[6] and is convenient for comparing the responsiveness of several drugs to a marker gene list. The disadvantages of this scoring system are that it overestimates responsiveness when the list contains a gene for which induction is extreme (such as CYP1A1) and it underestimates responsiveness when genes in the list are mobilized in either direction. To overcome these disadvantages, we used another score, TGP2, which is based on the size of the effects $g = |\mu_2 - \mu_1|/\sigma_{pooled}$, where

$$\sigma_{pooled} = \sqrt{\frac{(N_1-1)\sigma_1 + (N_2-1)\sigma_2^2}{(N_1+N_2-2)}}$$

To obtain an unbiased estimate of the effect size $d = c \times d$, where c is bias correction[7]

$$c = 1 - \frac{3}{4(N_1+N_2-2)-1}$$

The corrected effect size was calculated for each probe set in the marker gene list, summed, and divided by the number of probe sets in the list, and finally multiplied by 100 to obtain the TGP2 score used in the present study.

Results

Changes in rat livers in response to treatment with coumarin

We noted several pathological changes in rat livers after administration of coumarin (Table 1). Twenty-four hour after a single dose of coumarin, no abnormal morphological changes were observed by light microcopy (Figure 1a,b). However, histopathological changes became apparent with repeated administration of coumarin for 1 week or later in the highest dose group, and degenerative lesions, such as vacuolar degeneration and intracytoplasmic inclusion bodies, were evident at day 29 post-initiation of treatment (Figure 1c,d). From day 4 to day 29, single cell necrosis of hepatocytes was occasionally observed.

We next used electron microscopy to look for subtle changes that may be apparent 24 h after a single dose of coumarin. The analysis showed dilation of the rough endoplasmic reticulum of hepatocytes in

Table 1 Histopathological findings in rat livers treated with coumarin

Histopathological findings	*Time Point (days)*	*2*			*4*			*8*			*15*			*29*		
	Dose (mg/kg)	*15*	*50*	*150*	*15*	*50*	*150*	*15*	*50*	*150*	*15*	*50*	*150*	*15*	*50*	*150*
	Number of animals examined	*5*	*5*	*5*	*5*	*5*	*5*	*5*	*5*	*5*	*5*	*5*	*5*	*5*	*5*	*5*
Hepatocyte / Single cell necrosis		0	0	0	0	0	1	0	0	1	0	0	1	0	0	2
very slight							1			1			1			2
Hepatocyte / Inclusion body, intracytoplasmic		0	0	0	0	0	0	0	0	5	0	0	5	0	0	5
very slight										5			2			
slight													3			2
moderate																3
Hepatocyte, centrilobular / Hypertrophy		0	0	0	0	0	0	0	0	3	0	0	5	0	0	5
very slight										3			2			1
slight													3			4
Hepatocyte, centrilobular / Degeneration, vacuolar		0	0	0	0	0	0	0	0	0	0	0	3	0	0	5
very slight													2			
slight													1			5

Vehicle alone or coumarin 15, 50, or 150 mg/kg was administered orally to rats once daily for 1, 3, 7, 14, and 28 days, and the animals were euthanized 24 h after the last dosing, namely, on 2, 4, 8, 15, and 29 days ($n = 5$). The pathological change in the liver was graded into four categories: very slight, slight, moderate, and severe. The number of animals having the morphology at each grade is shown.

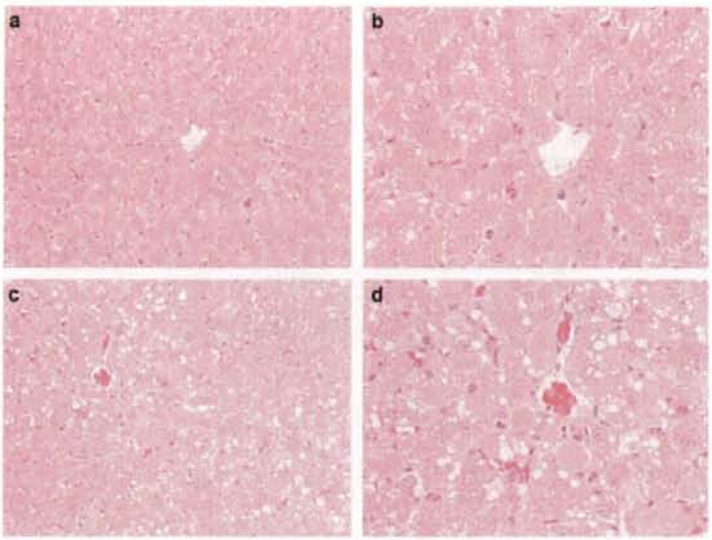

Figure 1 Histopathological changes in the rat liver treated with 150 mg/kg coumarin. (a) Low (×100) and (b) high (×200) magnification micrographs of a liver treated once with 150 mg/kg coumarin (24 h after a single dose). No abnormal morphological changes were detected in the control liver. (c) Low (×100) and (d) high (×200) magnification images of a liver treated with 150 mg/kg coumarin once a day for 28 days. Degenerative changes, such as vacuolation of hepatocytes, are evident after repeated administration of coumarin.

the centrilobular region of the liver in the highest dose group (Figure 2). This early slight ultrastructural change was considered to be consistent with hepatic injury we observed after repeated exposure to the drug. Thus, the 24-h post-treatment time point seemed appropriate for microarray analysis, as at the cellular level, coumarin had already begun exerting an effect at 24-h post-single treatment.

As described in the Methods section, statistically significant up- (136 probe sets) and down-regulated genes (79 probe sets) were extracted and these are listed in Tables 2 and 3. In livers treated with coumarin, the following genes were remarkably mobilized, that is, genes involved in glutathione metabolism and oxidative stress: "glutathione reductase", "glutathione-S-transferase, pi 1/2", "glutathione S-transferase Yc2 subunit", "microsomal glutathione S-transferase 2", "glutamate-cysteine ligase, catalytic subunit", "glutamate-cysteine ligase, modifier subunit", "aldo-keto reductase family 7, member A3

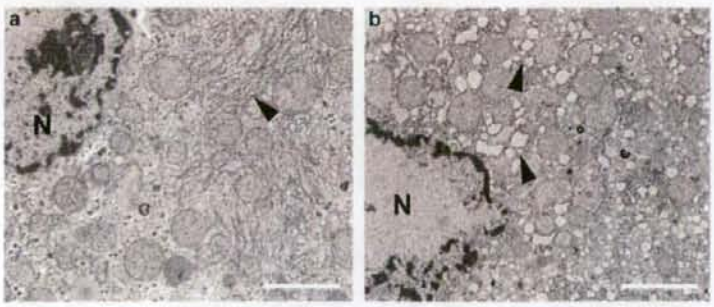

Figure 2 Early detection of coumarin-induced changes by electron microscopy. (a) Control hepatocyte, (b) coumarin-treated hepatocyte (150 mg/kg; 24 h after a single dose). Expansion of the rough endoplasmic reticulum (rER) in the coumarin-treated hepatocyte as compared with a control is evident. N, nucleus; Arrowhead, rER; Bar = 2 μm.

Table 2 Genes up-regulated in the rat liver 24 h after administration of coumarin

Affymetrix probe set ID	*Gene symbol*	*Gene description*	*Fold change*		
			Dose (mg/kg)		
			15	*50*	*150*
1371817_at	LOC290651	Similar to myo-inositol 1-phosphate synthase A1	9.52		26.50
1388122_at	Gstp1/Gstp2	Glutathione-S-transferase, pi 1/pi 2	2.84	1.57	13.00
1369698_at	Abcc3	ATP-binding cassette, sub-family C (CFTR/MRP), member 3	4.41	2.59	11.58
1370342_at	Kcnk2	Potassium channel, subfamily K, member 2	2.45	3.22	10.87
1368013_at	Ddit4l	DNA-damage-inducible transcript 4-like	1.71	1.41	9.07
1388271_at	LOC682651/LOC689415	Similar to Metallothionein-2 (MT-2) (Metallothionein-II) (MT-II)	1.39	1.40	8.81
1375213_at	Pck2_predicted	Phosphoenolpyruvate carboxykinase 2 (mitochondrial) (predicted)	3.07	1.97	6.09
1371237_a_at	Mt1a	Metallothionein 1a	1.52	1.70	5.92
1368121_at	Akr7a3	Aldo-keto reductase family 7, member A3 (aflatoxin aldehyde reductase)	3.43	2.00	5.78
1387599_a_at	Nqo1	NAD(P)H dehydrogenase, quinone 1	2.68	2.33	5.77
1371970_at	RGD1560913_predicted	Similar to expressed sequence AW413625 (predicted)	2.92	1.19	5.67
1371089_at	—	Transcribed locus	2.25	1.38	5.29
1379740_at	LOC361346	Similar to chromosome 18 open reading frame 54	2.29	2.32	4.96
1387693_a_at	Slc6a9	Solute carrier family 6 (neurotransmitter transporter, glycine), member 9	1.66	0.97	4.94
1372510_at	Srxn1	Sulfiredoxin 1 homolog	1.19	0.95	4.91
1370902_at	Akr1b8	Aldo-keto reductase family 1, member B8	2.20	1.96	4.69
1369772_at	Slc6a9	Solute carrier family 6 (neurotransmitter transporter, glycine), member 9	1.45	0.92	4.42
1368247_at	Hspa1a /Hspa1b	Heat shock 70kD protein 1A/1B (mapped)	2.18	1.94	4.22
1387925_at	Asns	Asparagine synthetase	1.40	1.35	4.06
1376051_at	Cryl1	Crystallin, lamda 1	1.25	1.24	3.94
1367847_at	Nupr1	Nuclear protein 1	1.24	1.46	3.86
1368143_at	Anxa7	Annexin A7	1.68	1.38	3.77
1377016_at	Creld2	Cysteine-rich with EGF-like domains 2	0.88	0.94	3.75
1373043_at	LOC680945/LOC683036	Similar to stromal cell–derived factor 2-like 1	1.86	1.99	3.71
1388102_at	Ltb4dh	Leukotriene B4 12-hydroxydehydrogenase	1.44	1.05	3.59
1372653_at	Fkbp11	FK506 binding protein 11	1.64	1.42	3.54
1373810_at	Pla2g12a_predicted	Phospholipase A2, group XIIA (predicted)	1.42	1.96	3.53
1376247_at	—	Transcribed locus	1.97	1.39	3.52
1371442_at	Hyou1	Hypoxia up-regulated 1	1.26	0.88	3.50
1372985_at	Zfp444_predicted	Zinc finger protein 444 (predicted)	2.10	1.28	3.47
1373787_at	Slc6a9	Solute carrier family 6 (neurotransmitter transporter, glycine), member 9	1.35	1.02	3.30
1394080_at	—	Transcribed locus	2.66	2.54	3.17
1373850_at	Smpdl3b	Sphingomyelin phosphodiesterase, acid-like 3B	1.46	1.23	3.07
1370073_at	Dnajc3	Protein kinase inhibitor p58	1.53	1.31	3.06
1374036_at	Mcm2_predicted	Minichromosome maintenance deficient 2 mitotin (predicted)	1.55	0.85	3.06
1370912_at	Hspa1b	Heat shock 70kD protein 1B (mapped)	1.64	1.46	3.01
1377145_at	LOC362068	Similar to monogenic, audiogenic seizure susceptibility 1	1.56	1.63	2.99
1392920_at	Ell3	Elongation factor RNA polymerase II-like 3	1.62	1.41	2.96
1376668_at	RGD1311126_predicted	Similar to RIKEN cDNA 4922503N01 (predicted)	0.92	0.79	2.94
1389308_at	Dnajb11	DnaJ (Hsp40) homolog, subfamily B, member 11	1.42	1.14	2.91
1376055_at	Mcm5_predicted	Minichromosome maintenance deficient 5, cell division cycle 46 (predicted)	1.81	1.07	2.90
1375852_at	Hmgcr	3-hydroxy-3-methylglutaryl-Coenzyme A reductase	1.28	0.91	2.90
1386958_at	Txnrd1	Thioredoxin reductase 1	1.07	0.81	2.89
1371210_s_at	RT1-Aw2	RT1 class Ib, locus Aw2	1.50	1.72	2.88
1372390_at	—	Transcribed locus	1.25	0.81	2.86
1374359_at	Ccne2_predicted	Cyclin E2 (predicted)	1.24	0.91	2.85
1370665_at	Hyou1	Hypoxia up-regulated 1	1.03	0.87	2.84
1387212_at	Bhlhb8	Basic helix-loop-helix domain containing, class B, 8	1.51	2.29	2.81
1374805_at	RGD1561749_predicted	Similar to hypothetical protein MGC5528 (predicted)	2.25	1.13	2.81
1389578_at	Isrip	Ischemia/reperfusion inducible protein	1.23	1.25	2.73
1370429_at	RT1-Aw2	RT1 class Ib, locus Aw2	1.89	1.29	2.70
1370803_at	Zwint	ZW10 interactor	1.58	1.23	2.68
1370688_at	Gclc	Glutamate-cysteine ligase, catalytic subunit	1.06	0.64	2.67
1377037_at	LOC679253/LOC681337	Similar to Acyl-coA thioesterase 4	1.32	0.96	2.65
1375428_at	Creg_predicted	Cellular repressor of E1A-stimulated genes (predicted)	1.24	1.17	2.65
1374048_at	Nrtn	Neurturin	1.61	1.63	2.64
1377334_at	RT1-Ba	RT1 class II, locus Ba	1.86	1.85	2.63

(continued)

Table 2 *(continued)*

Affymetrix probe set ID	*Gene symbol*	*Gene description*	*Fold change*		
			Dose (mg/kg)		
			15	*50*	*150*
1388628_at	Tmed3	Transmembrane emp24 domain containing 3	1.40	1.17	2.59
1367733_at	Ca2	Carbonic anhydrase 2	1.11	0.86	2.59
1373557_at	Mcm4	Minichromosome maintenance deficient 4 homolog	1.51	0.90	2.57
1368544_a_at	Nol3	Nucleolar protein 3	1.30	1.67	2.57
1372954_at	—	Sprague-Dawley UV73 mRNA, partial sequence	1.37	1.80	2.54
1369061_at	Gsr	Glutathione reductase	1.27	1.09	2.53
1370007_at	Pdia4	Protein disulfide isomerase associated 4	1.10	0.98	2.53
1389391_at	RGD1564876_predicted	Similar to solute carrier family 35, member E3 (predicted)	1.26	0.98	2.50
1372523_at	Gclc	Glutamate-cysteine ligase, catalytic subunit	1.17	0.79	2.50
1390591_at	Slc17a3	Na/Pi cotransporter 4	1.67	1.07	2.49
1368376_at	Nr0b2	Nuclear receptor subfamily 0, group B, member 2	1.74	1.69	2.49
1398791_at	Txnrd1	Thioredoxin reductase 1	1.10	0.89	2.48
1367938_at	Ugdh	UDP-glucose dehydrogenase	1.28	0.96	2.46
1387022_at	Aldh1a1	Aldehyde dehydrogenase family 1, member A1	2.15	1.21	2.44
1373613_at	LOC300191	Similar to RIKEN cDNA 4930570C03	1.09	0.96	2.44
1372406_at	Mcm3_predicted	Minichromosome maintenance deficient 3 (predicted)	1.65	0.81	2.43
1374121_at	—	Transcribed locus	2.32	1.82	2.41
1372261_at	—	Transcribed locus	1.23	1.13	2.41
1384130_at	RGD1560171_predicted	Similar to PRO0149 protein (predicted)	1.63	2.13	2.39
1380030_at	Znf593_predicted	Zinc finger protein 593 (predicted)	1.09	0.88	2.38
1389671_at	Trpc2	Transient receptor potential cation channel, subfamily C, member 2	1.21	1.29	2.36
1373445_at	Nol8_predicted	Nucleolar protein 8 (predicted)	1.24	0.85	2.36
1387083_at	Ctf1	Cardiotrophin 1	1.18	0.96	2.35
1377135_at	Alox5	Arachidonate 5-lipoxygenase	1.00	1.25	2.34
1375088_at	—	Transcribed locus	0.98	1.14	2.31
1369588_a_at	Atpif1	ATPase inhibitory factor 1	1.27	1.13	2.30
1398341_at	RGD1559720_predicted	RGD1559720 (predicted)	1.03	1.09	2.29
1389767_at	RGD1304924_predicted	Similar to hypothetical protein FLJ31364 (predicted)	1.13	1.18	2.29
1374249_at	RGD1304580	Similar to Hypothetical protein MGC38513	0.93	1.10	2.28
1373530_at	Ccne1	cyclin E	1.06	0.52	2.28
1371113_a_at	Tfrc	Transferrin receptor	1.28	0.76	2.28
1370127_at	Pold1	Polymerase (DNA directed), delta 1, catalytic subunit	1.42	1.37	2.28
1376073_at	Sel1h	Sel1 (suppressor of lin-12) 1 homolog	1.40	1.06	2.26
1392841_at	—	Transcribed locus	1.39	2.02	2.23
1398879_at	Tmem66	Transmembrane protein 66	1.25	1.07	2.22
1388622_at	Nol5a	Nucleolar protein 5A	1.46	1.19	2.22
1371583_at	Rbm3	RNA binding motif protein 3	1.19	1.16	2.21
1387188_at	Slc17a1	Solute carrier family 17, member 1	1.37	1.33	2.20
1368037_at	Cbr1	Carbonyl reductase 1	0.96	1.01	2.20
1390430_at	Nr1d2	Nuclear receptor subfamily 1, group D, member 2	0.97	1.05	2.19
1398788_at	Pdia3	Protein disulfide isomerase associated 3	1.43	1.24	2.19
1386922_at	Ca2	Carbonic anhydrase 2	1.07	0.83	2.19
1367983_at	Fen1	Flap structure-specific endonuclease 1	1.59	1.12	2.16
1373999_at	—	Transcribed locus	1.27	0.83	2.16
1376781_at	Glb1_mapped	Galactosidase, beta 1 (mapped)	1.20	1.03	2.14
1381968_at	Sema6d_predicted	Sema domain, transmembrane domain (TM), and cytoplasmic domain, (semaphorin) 6D (predicted)	1.18	1.20	2.13
1372774_at	Coq6	Coenzyme Q6 homolog	1.30	0.90	2.13
1376098_a_at	Lad1_predicted	Ladinin (predicted)	1.02	1.03	2.12
1370904_at	Hla-dma	Major histocompatibility complex, class II, DM alpha	1.32	1.11	2.12
1389805_at	—	—	1.27	1.29	2.11
1388331_at	Tra1_predicted	Tumor rejection antigen gp96 (predicted)	1.08	0.93	2.11
1386466_at	—	Transcribed locus	1.08	1.24	2.11
1372599_at	Mgst2_predicted	Microsomal glutathione S-transferase 2 (predicted)	1.34	1.34	2.11
1372471_at	—	Transcribed locus	1.66	1.03	2.10
1372247_at	Ddost_predicted	Dolichyl-di-phosphooligosaccharide-protein glycotransferase (predicted)	1.26	1.15	2.10
1370055_at	Rab3d	RAB3D, member RAS oncogene family	0.72	0.77	2.10
1398596_at	—	Transcribed locus	2.07	1.65	2.09
1387783_a_at	Acaa1	Acetyl-coenzyme A acyltransferase 1	1.49	1.20	2.09
1373908_at	—	—	1.71	1.40	2.09
1398383_at	Cyb561_predicted	Cytochrome b-561 (predicted)	1.40	1.15	2.07
1377350_at	—	Transcribed locus	1.74	1.26	2.07
1370428_x_at	RT1-Aw2	RT1 class Ib, locus Aw2	1.66	1.50	2.07

(continued)

Table 2 *(continued)*

Affymetrix probe set ID	*Gene symbol*	*Gene description*	*Fold change*		
			Dose (mg/kg)		
			15	*50*	*150*
1369693_a_at	Slc1a2	Solute carrier family 1, member 2	1.81	1.96	2.07
1370541_at	Nr1d2	Nuclear receptor subfamily 1, group D, member 2	0.91	1.01	2.06
1389004_at	Josd2_predicted	Josephin domain containing 2 (predicted)	1.12	0.95	2.06
1370030_at	Gclm	Glutamate cysteine ligase, modifier subunit	1.06	0.81	2.06
1370000_at	Thra	Thyroid hormone receptor alpha	1.79	1.66	2.06
1370663_at	Wee1	Wee 1 homolog	1.92	1.00	2.05
1390321_at	RGD1304693_predicted	Similar to CG14803-PA (predicted)	1.68	1.15	2.03
1389209_at	RGD1306274	Similar to hypothetical protein BC002942	1.82	1.17	2.03
1388750_at	Tfrc	Transferrin receptor	1.32	0.87	2.03
1373935_at	Pold2	Polymerase (DNA directed), delta 2, regulatory subunit	1.35	1.18	2.03
1390579_at	RGD1305222_predicted	Similar to RIKEN cDNA 1810029B16 (predicted)	0.84	0.70	2.02
1389889_at	RGD1306404_predicted	Similar to mKIAA1402 protein (predicted)	1.21	1.03	2.02
1373499_at	Gas5	Growth arrest specific 5	1.15	1.03	2.02
1373386_at	Gjb2	Gap junction membrane channel protein beta 2	0.81	1.08	2.02
1376001_at	Praf1_predicted	Polymerase (RNA) I associated factor 1 (predicted)	1.17	0.98	2.01
1373200_at	Eef1e1_predicted	Eukaryotic translation elongation factor 1 epsilon 1 (predicted)	1.19	1.25	2.01
1380854_at	R3hdm1	R3H domain containing 1	1.20	1.28	2.00

Probe sets are sorted by fold change. Shaded probe sets, those selected as in-vivo–in-vitro bridging probes (see Figure 3).

(aflatoxin aldehyde reductase)", "NAD(P)H dehydrogenase, quinone 1", "thioredoxin reductase 1", and "metallothionein"; genes related to the heat shock response: "crystallin, lamda 1", "DnaJ (Hsp40) homolog, subfamily B, member 11", "heat shock 70kD protein 1A/1B", and "protein kinase inhibitor p58"; genes responsive to hypoxia: "hypoxia up-regulated 1" and "ischemia/reperfusion inducible protein"; and genes related to DNA repair and the cell cycle: "DNA-damage-inducible transcript 4-like", "cyclin E", "growth arrest specific 5", and "wee 1 homolog". Changes in expression of these genes in hepatocytes can be interpreted as a reflection of the adaptive response to oxidative stress and cellular damage. Among the extracted genes, the following genes appeared to be the most sensitive to coumarin, "aldo-keto reductase family 7, member A3", "NAD(P)H dehydrogenase, quinone 1", "glutathione reductase", "glutathione-S-transferase, pi 1/2", and "glutathione S-transferase Yc2 subunit", as they were remarkably mobilized at the lowest dose of coumarin-treatment (15 mg/kg).

Comparison between in-vivo and in-vitro rat hepatocyte responses

Primary cultured rat hepatocytes were exposed to 12, 60, and 300 μM coumarin for 24 h. No obvious cytotoxicity was detected by LDH release (100.5, 97.7, and 95.1% of control, respectively). In case of the in-vitro system, statistical filtering was not appropriate because the data were the duplicate measurements from a single rat. We then extracted the significant genes according to the gene list obtained from in-vivo study, that is, the genes showing significant up- (136 probe sets) or down-regulation (79 probe sets) in livers treated with 150 mg/kg coumarin. As shown in Figure 3a, a similar trend was observed between in-vivo and in-vitro cell responses, although the extent of the response (i.e., fold change) was generally smaller, and fewer genes showed a measurable change in the in-vitro cell assay. Probe sets showing changes of 1.5-fold or more and 0.6-fold or less than that of control at the highest concentration (300 μM) in rat hepatocytes were selected as those reflecting the toxicological mechanism of coumarin *in vivo*, namely, "in-vivo–in-vitro bridging probes". For the selected genes (37 up-regulated and 29 down-regulated; see shading in Tables 2 and 3), clear dose-dependent changes in expression were observed (Figure 3b), and the observation enabled us to assess hepatotoxicity of coumarin using the in-vitro data.

Comparison between rat and human hepatocytes

Cultured human hepatocytes were also exposed to 12, 60, and 300 μM coumarin for 24 h. No obvious cytotoxicity was detected by LDH release (100.6, 100.9, and 102.0% of control, respectively). The in-vivo–in-vitro bridging probes were assigned to their human ortholog genes to form a set of "rat–human bridging probes" and changes in their expression were compared in rat versus human hepatocytes. In total, 14 up-regulated and 11 down-regulated probe sets were identified and their relative expression levels are shown as a heatmap in Figure 4. It appears that the pattern of changes in gene expres-

Table 3 Genes down-regulated in the rat liver 24 h after administration of coumarin

Affymetrix probe set ID	*Gene symbol*	*Gene description*	*Fold change*		
			Dose (mg/kg)		
			15	*50*	*150*
1386977_at	Ca3	Carbonic anhydrase 3	0.64	1.01	0.13
1370778_at	LOC259245	Alpha-2u globulin	0.87	0.84	0.16
1386474_at	—	Transcribed locus	1.53	0.59	0.19
1393902_at	Akr1c6	Aldo-keto reductase family 1, member C6	0.42	0.53	0.20
1375900_at	LOC500590	Similar to T-cell antigen 4-1BB precursor – mouse	0.56	0.52	0.21
1371412_a_at	Nrep	Neuronal regeneration related protein	0.86	0.88	0.25
1387491_at	Gyk	Glycerol kinase	0.76	0.72	0.28
1376637_at	—	Transcribed locus	0.62	1.03	0.29
1373722_at	Kif20a_predicted	Kinesin family member 20A (predicted)	1.12	0.91	0.29
1367896_at	Ca3	Carbonic anhydrase 3	0.80	0.98	0.29
1385247_at	Ugt2b	UDP glycosyltransferase 2 family, polypeptide B	0.68	0.04	0.31
1387852_at	Thrsp	Thyroid hormone–responsive protein	1.06	0.87	0.32
1393221_at	RGD1564865_predicted	Similar to 20-alpha-hydroxysteroid dehydrogenase (predicted)	0.67	0.97	0.32
1387665_at	Bhmt	Betaine-homocysteine methyltransferase	0.81	1.18	0.33
1387185_at	Apbb3	Amyloid beta (A4) precursor protein-binding, family B, member 3	0.84	0.84	0.33
1387053_at	Fmo1	Flavin containing monooxygenase 1	0.62	0.79	0.34
1398286_at	Csad	Cysteine sulfinic acid decarboxylase	1.07	0.92	0.34
1387655_at	Cxcl12	Chemokine (C-X-C motif) ligand 12	0.67	0.45	0.34
1368458_at	Cyp7a1	Cytochrome P450, family 7, subfamily a, polypeptide 1	0.78	0.69	0.36
1388583_at	Cxcl12	Chemokine (C-X-C motif) ligand 12	0.77	0.67	0.37
1387243_at	Cyp1a2	Cytochrome P450, family 1, subfamily a, polypeptide 2	0.78	0.90	0.37
1387139_at	Hao2	Hydroxyacid oxidase 2 (long chain)	0.79	1.15	0.37
1373006_at	Prp2	Proline-rich protein PRP2	0.70	0.79	0.37
1370026_at	Cryab	Crystallin, alpha B	1.01	0.71	0.37
1390443_at	—	Transcribed locus	0.88	0.75	0.38
1375144_at	—	Transcribed locus	1.02	0.52	0.39
1369044_a_at	Pde4b	Phosphodiesterase 4B	0.59	0.64	0.39
1370057_at	Csrp1	Cysteine and glycine-rich protein 1	0.93	0.90	0.39
1369450_at	Ust5r	Integral membrane transport protein UST5r	0.74	0.94	0.39
1367729_at	Oat	Ornithine aminotransferase	0.63	1.00	0.39
1374677_at	LOC684425	Similar to adenylosuccinate synthetase isozyme 1	0.80	1.00	0.40
1388038_at	Atrn	Attractin	0.88	0.88	0.40
1388031_x_at	LOC259245/Mup5	Alpha-2u globulin	0.70	0.95	0.40
1370150_a_at	Thrsp	Thyroid hormone–responsive protein	1.03	0.97	0.41
1390450_a_at	Ogn_predicted	Osteoglycin (predicted)	0.63	0.53	0.41
1369664_at	Avpr1a	Arginine vasopressin receptor 1A	0.88	0.87	0.41
1388433_at	Krt1-19	Keratin complex 1, acidic, gene 19	1.09	0.71	0.42
1371400_at	Thrsp	Thyroid hormone–responsive protein	1.04	0.98	0.42
1369296_at	Sult1c1	Sulfotransferase family, cytosolic, 1C, member 1	0.86	1.13	0.42
1389728_at	—	—	0.77	0.56	0.42
1389188_at	Gpr108	G protein-coupled receptor 108	0.69	0.53	0.42
1380546_at	LOC298250	Similar to hypothetical protein FLJ10986	0.87	0.89	0.42
1376427_a_at	Gldc_predicted	Glycine decarboxylase (predicted)	0.85	0.88	0.42
1372685_at	Cdkn3_predicted	Cyclin-dependent kinase inhibitor 3 (predicted)	1.03	1.14	0.42
1369546_at	Bbox1	Butyrobetaine (gamma), 2-oxoglutarate dioxygenase 1	0.90	0.82	0.42
1389566_at	Ccnb2	Cyclin B2	1.13	1.11	0.43
1374157_at	Rgs8	Regulator of G-protein signaling 8	0.76	0.61	0.43
1398282_at	Kynu	Kynureninase (L-kynurenine hydrolase)	0.73	0.96	0.44
1387816_at	Igfals	Insulin-like growth factor binding protein, acid labile subunit	1.09	0.77	0.45
1387528_at	Mbl2	Mannose binding lectin 2, protein C	0.77	0.86	0.45
1387372_at	Slc6a13	Solute carrier family 6, member 13	0.89	0.75	0.45
1376311_at	RGD1563465_predicted	Similar to netrin G1 (predicted)	0.79	0.29	0.45
1374072_at	LOC689898	Hypothetical protein LOC689898	0.97	0.62	0.45
1370355_at	Scd1	Stearoyl-coenzyme A desaturase 1	1.56	1.13	0.45
1368627_at	Rgn	Regucalcin	0.85	0.91	0.45
1387203_at	Gckr	Glucokinase regulatory protein	0.79	1.01	0.46
1388425_at	RGD1305890	Similar to RIKEN cDNA D130038B21	0.83	0.78	0.46
1377412_at	—	Transcribed locus	0.91	0.67	0.46
1377375_at	Aass_predicted	Aminoadipate-semialdehyde synthase (predicted)	0.98	0.80	0.46
1374760_at	—	Transcribed locus	0.76	1.07	0.46
1373967_at	—	Transcribed locus	0.87	0.77	0.46
1367979_s_at	Cyp51	Cytochrome P450, subfamily 51	0.92	0.77	0.46
1367939_at	Rbp1	Retinol binding protein 1, cellular	0.62	0.90	0.46

(continued)

Table 3 *(continued)*

Affymetrix probe set ID	*Gene symbol*	*Gene description*	*Fold change*		
			Dose (mg/kg)		
			15	*50*	*150*
1394068_x_at	Klf2_predicted	Kruppel-like factor 2 (lung) (predicted)	0.74	0.70	0.47
1389681_at	Pvrl2	Poliovirus receptor-related 2	0.88	0.97	0.47
1387307_at	Hal	Histidine ammonia lyase	0.87	0.76	0.47
1373814_at	RGD1310066	Similar to mKIAA1002 protein	0.80	0.84	0.47
1390672_at	Rprm	Candidate mediator of the p53-dependent G2 arrest	0.83	0.79	0.48
1367857_at	Fads1	Fatty acid desaturase 1	1.06	0.93	0.48
1387328_at	Cyp2c	Cytochrome P450, subfamily IIC (mephenytoin 4-hydroxylase)	0.80	1.06	0.48
1386975_at	Pdk2	Pyruvate dehydrogenase kinase, isoenzyme 2	0.61	0.65	0.48
1376785_at	Sycp3	Synaptonemal complex protein 3	0.70	0.85	0.48
1367804_at	Apcs	Serum amyloid P-component	0.70	0.78	0.48
1398759_at	Tgfb1i4	Transforming growth factor beta 1 induced transcript 4	0.72	0.83	0.49
1386041_a_at	Klf2_predicted	Kruppel-like factor 2 (lung) (predicted)	0.83	0.63	0.49
1375599_at	Ddx31_predicted	DEAD/H (Asp-Glu-Ala-Asp/His) box polypeptide 31 (predicted)	0.86	0.57	0.49
1388300_at	Mgst3_predicted	Microsomal glutathione S-transferase 3 (predicted)	0.69	1.00	0.50
1368733_at	Ste	Sulfotransferase, estrogen preferring	0.88	0.98	0.50
1368227_at	Slc28a2	Solute carrier family 28, member 2	1.05	0.84	0.50

Probe sets are sorted by fold change. Shaded probe sets are the ones selected as in-vivo–in-vitro bridging probes (see Figure 3).

sion is similar in rat and human cells but that the extent of the changes is more prominent in rat cells than in human cells. Among them, "protein kinase inhibitor p58", "DnaJ (Hsp40) homolog, subfamily B, member 11", "crystallin, lamda 1", "hypoxia up-regulated 1", and "aldo-keto reductase family 7, member A3 (aflatoxin aldehyde reductase)", which showed remarkable expression changes both in rat *in vivo* and *in vitro*, did not show any significant changes in human hepatocytes. As for the genes such as "ischemia/reperfusion inducible protein", "glutathione reductase", "glutamate-cysteine ligase, catalytic subunit", "NAD(P)H dehydrogenase, quinone 1", and "DNA-damage-inducible transcript 4-like", these were up-regulated in both species, but the extent of up-regulation was much less in human cells than in the rat.

In the next step, changes in expression of these were examined in cells treated with another hepatotoxicant, DFNa, which is known to elicit a similar response as does coumarin, that is, oxidative stress and glutathione depletion.[8,9] Although not all the genes showed changes in common with those observed after coumarin treatment, the trend appeared similar, suggesting that both compounds share the same toxicological pathway(s).

To make a quantitative comparison of responsiveness of the marker genes between species, the mean value of the effect size of the probe sets (TGP2 score) was calculated (Figure 5). It is obvious from the results presented in Figure 5a that the score shows a good dose-dependency, suggesting that the score successfully expresses the responsiveness of cells to the toxicant. Moreover, in the case of coumarin, the score of human hepatocytes to the marker genes is a much lower value than the score observed for rat cells, supporting the known species-specific difference. However, both rat and human cells responded to the markers to the same extent at the same concentration of DFNa. For genes such as "ischemia/reperfusion inducible protein" and "hypoxia up-regulated 1", these were up-regulated in both species at a high-dose DFNa exposure (data not shown). This clearly indicates that the marker genes respond similarly in rat and human hepatocytes when a drug with a similar level of toxicity in each species is applied.

Discussion

Coumarin is a toxin found in many plants, including the tonka bean, and it has clinical value as the precursor for several anticoagulants, especially warfarin. Although coumarin has a sweet scent, its use as a food additive is restricted because of its hepatotoxicity. It is well known that coumarin is a non-genotoxic hepatocarcinogen in rats, whereas such a property has not been probed in other species.[10] The mechanism of coumarin toxicity has been extensively studied and elucidated; it produces oxidative stress leading to glutathione depletion.[11–13] The species-specific difference between rat and human responses to coumarin has been explained as a difference in detoxification after metabolic activation.[14,15]

In most species, including humans, coumarin is hydroxylated by CYP2A to 7-hydroxycoumarin

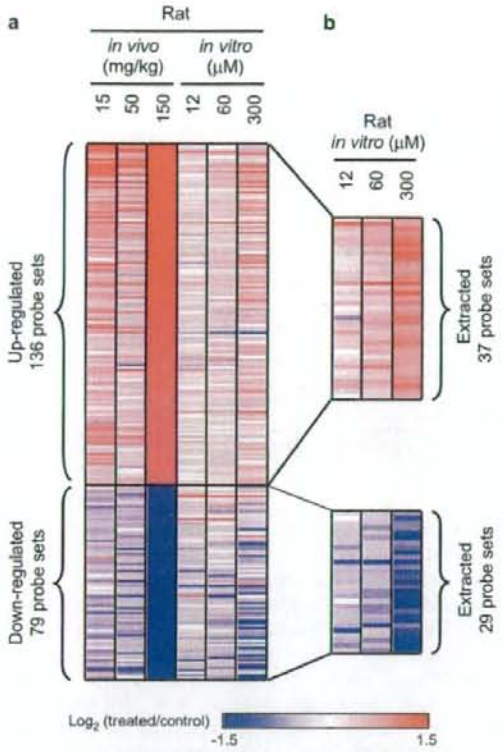

Figure 3 Heatmap of the expression profiles of probe sets in rat liver and rat hepatocytes treated with coumarin. (a) Heatmap of the changes in gene expression induced by coumarin treatment in the in-vivo rat liver (15, 50, 150 mg/kg) and in-vitro hepatocytes (12, 60, and 300 μM). Probes sets were statistically extracted from the data presented in Tables 2 and 3. b: Probe sets with >1.5-fold or <0.6-fold change in rat hepatocytes (the specific sub-set grouped as in-vivo–in-vitro bridging probes are indicated by shading in Tables 2 and 3).

(7-HC), a non-toxic metabolite. In rats, however, CYP2A has a stronger affinity for testosterone than for coumarin, such that 7HC levels are extremely low in this species. Another influencing factor is that in rats, coumarin is converted to coumarin 3,4-epoxide (CE), a reactive intermediate that is detoxified via glutathione conjugation and excreted as a conjugate. When the amount of the active metabolite exceeds the cellular capacity for glutathione conjugation, cell injury may occur. However, there is some evidence to suggest that this pathway is of minor importance to hepatotoxicity, as mouse-liver microsomes show hepatic clearance of coumarin via the epoxide intermediate at levels four times greater than that in rats,[16] but hepatotoxicity is not induced by coumarin treatment in mice. CE is spontaneously converted to another toxic compound, *o*-hydroxyphenylacetaldehyde (*o*-HPA). It has been found that *o*-HPA is rapidly detoxified to *o*-hydroxyphenylacetic acid in mice and humans, whereas this pathway works little in rats.[16,17] Therefore, the difference in *o*-HPA detoxification is currently considered to be the main cause of species-specific differences in sensitivity to coumarin.

The main purpose of the present study was to explore a possible strategy for overcoming the problem of species-specific differences in toxicity that affect testing of potential toxins and therapeutic treatments. Specifically, we were interested to test a toxicogenomics-based approach to address species-specific differences in response to toxins. In the livers of rats treated with coumarin, changes in gene expression were observed in various known genes, possibly reflecting a response to oxidative stress, cell injury, and glutathione depletion, and these coumarin-responsive genes seem likely to be related to the hepatotoxic mechanism of coumarin. Of the coumarin-responsive gene identified in the in-vivo rat liver assay, not all but a considerable numbers of the genes were found to be common to those that were coumarin-responsive in the in-vitro assay, with an observable dose-dependency. The present results suggest that whole-transcriptome analysis of the response can be used to estimate the hepatotoxicity of coumarin using the in-vitro rat hepatocytes. In our experience with other compounds, we found that some chemicals showed a considerably different gene expression profile *in vivo* and *in vitro*,[6] whereas the results with coumarin suggest that it is possible to build a reasonable bridge between rat and human responses using an in-vitro cell assay system.

The responsive genes in common to the in-vivo and in-vitro assay datasets were used to identify human ortholog genes useful for making a comparison between rat and human responses. As it is obvious from the results presented in Figure 4, the trend in changes in expression was similar in both species, but the extent of the changes was generally smaller in human cells than in rat cells in accordance with the known species-specific difference in hepatotoxicity. The observation that induction of stress-related genes and glutathione metabolism–related genes was more robust in rat cells than in human cells could be a direct reflection of the extent of stress and subsequent damage caused by coumarin in each species. The genes "Protein kinase inhibitor p58", "DnaJ (Hsp40) homolog, subfamily B, member 11", "crystallin, lamda 1", "hypoxia up-regulated 1", and "aflatoxin aldehyde reductase" were extensively

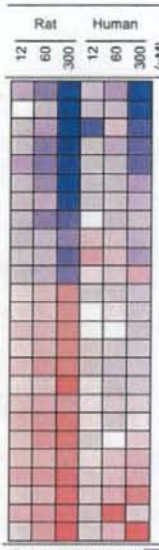

Affymetrix probe ID			
RAE230 2.0	HG-U133 2.0	Gene description (RAE230 2.0)	Gene symbol
1387053_at	205666_at	flavin containing monooxygenase 1	Fmo1
1387243_at	207608_x_at	cytochrome P450, family 1, subfamily A, polypeptide 2	Cyp1a2
1367896_at	204865_at	carbonic anhydrase 3	Ca3
1387139_at	231156_at	hydroxyacid oxidase 2 (long chain)	Hao2
1388583_at	203666_at	chemokine (C-X-C motif) ligand 12	Cxcl12
1387816_at	215712_s_at	insulin-like growth factor binding protein, acid labile subunit	Igfals
1387852_at	229477_at	thyroid hormone responsive protein	Thrsp
1387665_at	206119_at	betaine-homocysteine methyltransferase	Bhmt
1387528_at	207256_at	mannose-binding lectin 2, protein C	Mbl2
1369044_a_at	211302_s_at	phosphodiesterase 4B	Pde4b
1367857_at	208962_s_at	fatty acid desaturase 1	Fads1
1370073_at	208499_s_at	protein kinase inhibitor p58	Dnajc3
1389308_at	223054_at	DnaJ (Hsp40) homolog, subfamily B, member 11	Dnajb11
1390591_at	207298_at	Na/Pi cotransporter 4	Slc17a3
1370665_at	200825_s_at	hypoxia up-regulated 1	Hyou1
1368121_at	206469_x_at	aldo-keto reductase family 7, member A3 (aflatoxin aldehyde reductase)	Akr7a3
1376051_at	220753_s_at	crystallin, lamda 1	Cryl1
1370688_at	202922_at	glutamate-cysteine ligase, catalytic subunit	**Gclc**
1389578_at	218647_s_at	ischemia/reperfusion inducible protein	Yrdc
1369061_at	225609_at	glutathione reductase	Gsr
1373810_at	223373_s_at	phospholipase A2, group XIIA (predicted)	Pla2g12a
1387599_a_at	201468_s_at	NAD(P)H dehydrogenase, quinone 1	Nqo1
1370902_at	206561_s_at	aldo-keto reductase family 1, member B8	Akr1b8
1368013_at	228057_at	DNA-damage-inducible transcript 4-like	**Ddit4l**
1368247_at	200800_s_at	heat shock 70kD protein 1A/1B	**Hspa1a/1b**

Figure 4 Heatmap of the expression profile of probe sets in rat and human hepatocytes treated with coumarin. Among the set of in-vivo–in-vitro bridging probes for rats, 14 up-regulated and 11 down-regulated probe sets were assigned human orthologs (species bridging markers) and their expression is shown as a heatmap that includes the expression profiles in rat and human hepatocytes treated with 12, 60, or 300 μM coumarin. Note that each probe set responded dose-dependently to coumarin in both species, whereas the extent of the changes appears to be more prominent in rat than in human cells.

up-regulated in rats both *in vivo* and *in vitro*, whereas almost no change was observed in these genes in human hepatocytes. It will likely be interesting to determine if the gene sets include genes involved in the cause of the species-specific responses that lead to differences in hepatotoxicity and those genes not involved in the response to coumarin. Clearly, it will be necessary to perform additional experiments to address this question.

We next explored the utility of a score, the TGP2-score that is aimed at quantifying responsiveness of a set of marker genes. The TGP2-score is the average of the effect size on gene expression. When species-specific differences in drug-induced gene expression changes are examined, we often encounter clusters of genes, possibly related to toxicological function, that are affected by the drug in both species tested but in different directions (i.e., up-regulated in one but down-regulated in the other). If responsiveness is quantified by taking account of the direction of changes, we might underestimate the extent to which the set of genes affected are similar. Using the TGP2-score, we estimate responsiveness of a given species when expression of a gene in the analysis set is mobilized in either direction. In the present case, however, the direction of expression change was in common between two species in most or all cases, such that the factor did not contribute much to the scores. The score is also clearly useful to visualize quantitative responsiveness of a set of genes to a toxicant (Figure 5) and a prediction of species-specific difference can also be represented (i.e., the higher toxicity of coumarin in rat than in humans or the lack of a species-specific difference in the case of toxicity of DFNa; Figure 5). It also follows that the genes selected in this study may be useful in-vitro markers of oxidative stress–related hepatocyte injury in both rats and humans and that differential responses in these marker genes are indicative of a species-specific difference.

In conclusion, we successfully used a toxicogenomics approach to reproduce the known species-specific difference in hepatotoxicity of coumarin between rats and humans using an in-vitro hepatocyte culture system and microarray analysis. The application of this approach to other chemicals in our database should reveal other examples that can build bridges between species or suggest other strategies for bridging information among species. The most important mission for a toxicologist interested

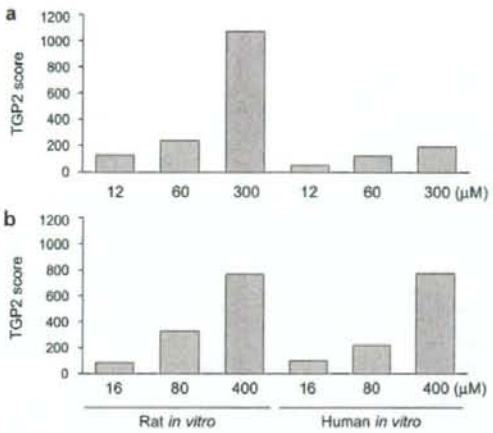

Figure 5 The responsiveness of rat and human hepatocytes expressed as a score based on the effect size (TGP2 score). The expression of each probe set in the set of rat–human bridging probes (Figure 4) was converted to a TGP2 score as described in "Materials and methods" to quantify the responsiveness of each species. (a) Responsiveness to coumarin. Note that the score shows a clear dose-dependency and the expected species-specific difference, that is, rat hepatocytes are more sensitive than human hepatocytes. (b) Responsiveness to diclofenac sodium, a known hepatotoxicant that causes oxidative stress but does not show a species-specific difference in hepatotoxicity. Again, a dose-dependent increase in the score is observed but in this case, as expected, no species-specific difference is observed.

in drug development is to make a precise prediction of the potential clinical toxicity based on animal studies. Toxicogenomics-based approaches are emerging as a promising new avenue of study for making the most of the results of animal studies.

Acknowledgement

This study was supported by a grant from the Ministry of Health, Labour and Welfare of Japan (H14-toxico-001).

References

1 Urushidani, T, Nagao, T. Toxicogenomics: the Japanese initiative. In: Borlak, J, (Ed.), *Handbook of toxicogenomics – strategies and applications. Wiley: VCH*; 2005. p. 623–31.
2 Takashima, K, Mizukawa, Y, Morishita, K, Okuyama, M, Kasahara, T, Toritsuka, N, *et al.* Effect of the difference in vehicles on gene expression in the rat liver-analysis of the control data in the Toxicogenomics Project Database. *Life Sci* 2006; **78**: 2787–2796.
3 Waters, MD, Fostel, JM. Toxicogenomics and systems toxicology: aims and prospects. *Nat Rev Genet* 2004; **5**: 936–948.
4 Mattingly, CJ, Colby, GT, Forrest, JN, Boyer, JL. The Comparative Toxicogenomics Database (CTD). *Environ Health Perspect* 2003; **111**: 793–795.
5 Liu, G, Loraine, AE, Shigeta, R, Cline, M, Cheng, J, Valmeekam, V, *et al.* NetAffx: Affymetrix probesets and annotations. *Nucleic Acids Res* 2003; **31**: 82–86.
6 Kiyosawa, N, Shiwaku, K, Hirode, M, Omura, K, Uehara, T, Shimizu, T, *et al.* Utilization of a one-dimensional score for surveying chemical-induced changes in expression levels of multiple biomarker gene sets using a large-scale toxicogenomics database. *J Toxicol Sci* 2006; **31**: 433–448.
7 Hedges, LV. Distribution theory for Glass's estimator of effect size and related estimators. *J Edu Statis* 1981; **6**: 107–128.
8 Gomez-Lechon, MJ, Ponsoda, X, O'Connor, E, Donato, T, Castell, JV, Jover, R. Diclofenac induces apoptosis in hepatocytes by alteration of mitochondrial function and generation of ROS. *Biochem Pharmacol* 2003; **66**: 2155–2167.
9 Amin, A, Hamza, AA. Oxidative stress mediates drug-induced hepatotoxicity in rats: a possible role of DNA fragmentation. *Toxicology* 2005; **208**: 367–375.
10 National Toxicology Program. NTP toxicology and carcinogenesis studies of coumarin (CAS No. 91-64-5) in F344/N rats and B6C3F1 mice (Gavage Studies). *Natl Toxicol Program Tech Rep Ser* 1993; **422**: 1–340.
11 Lake, BG. Investigations into the mechanism of coumarin-induced hepatotoxicity in the rat. *Arch Toxicol Suppl* 1984; **7**: 16–29.
12 Lake, BG, Gray, TJ, Evans, JG, Lewis, DF, Beamand, JA, Hue, KL. Studies on the mechanism of coumarin-induced toxicity in rat hepatocytes: comparison with dihydrocoumarin and other coumarin metabolites. *Toxicol Appl Pharmacol* 1989; **97**: 311–323.
13 Kiyosawa, N, Uehara, T, Gao, W, Omura, K, Hirode, M, Shimizu, T, *et al.* Identification of glutathione depletion-responsive genes using phorone-treated rat liver. *J Toxicol Sci* 2007; **32**: 469–486.
14 Vassallo, JD, Hicks, SM, Daston, GP, Lehman-McKeeman, LD. Metabolic detoxification determines species differences in coumarin-induced hepatotoxicity. *Toxicol Sci* 2004; **80**: 249–257.
15 Felter, SP, Vassallo, JD, Carlton, BD, Daston, GP. A safety assessment of coumarin taking into account species-specificity of toxicokinetics. *Food Chem Toxicol* 2006; **44**: 462–475.
16 Born, SL, Hu, JK, Lehman-McKeeman, LD. o-hydroxyphenylacetaldehyde is a hepatotoxic metabolite of coumarin. *Drug Metab Dispos* 2000a; **28**: 218–223.
17 Born, SL, Caudill, D, Smith, BJ, Lehman-McKeeman, LD. In vitro kinetics of coumarin 3,4-epoxidation: application to species differences in toxicity and carcinogenicity. *Toxicol Sci* 2000b; **58**: 23–31.

Biomaterials 29 (2008) 2719–2728

Contents lists available at ScienceDirect

Biomaterials

journal homepage: www.elsevier.com/locate/biomaterials

The slow resorption with replacement by bone of a hydrothermally synthesized pure calcium-deficient hydroxyapatite

Takatoshi Okuda [a,b], Koji Ioku [c], Ikuho Yonezawa [b], Hideyuki Minagi [d], Yoshinori Gonda [a,b], Giichiro Kawachi [c,1], Masanobu Kamitakahara [c], Yasuaki Shibata [a], Hisashi Murayama [e], Hisashi Kurosawa [b], Tohru Ikeda [a,*]

[a] Department of Oral Pathology and Bone Metabolism, Unit of Basic Medical Sciences, Nagasaki University Graduate School of Biomedical Sciences, 1-7-1 Sakamoto, Nagasaki 852-8588, Japan
[b] Department of Orthopedic Surgery, School of Medicine, Juntendo University, 2-1-1 Hongo, Bunkyo-ku, Tokyo 113-8421, Japan
[c] Graduate School of Environmental Studies, Tohoku University, 6-6-20 Aramaki, Aoba-ku, Sendai, Miyagi 980-8579, Japan
[d] Technical Research Laboratory, Toyo Kohan Co. Ltd., Kudamatsu, Yamaguchi 744-8611, Japan
[e] Kureha Special Laboratory Co. Ltd., 3-26-2 Hyakunin-cho, Shinjuku-ku, Tokyo 169-8503, Japan

ARTICLE INFO

Article history:
Received 18 February 2008
Accepted 18 March 2008
Available online 9 April 2008

Keywords:
Bone substitute
Biodegradation
Bone graft
Cell culture
Osteoclast

ABSTRACT

A newly developed calcium-deficient hydroxyapatite composed of rod-shaped particles synthesized by the hydrothermal method (HHA) and stoichiometric hydroxyapatite (SHA) synthesized by the sintering method was used for in vivo implantation and in vitro culture systems to compare these biological responses. In the rabbit femur, implanted HHA was slowly resorbed and about 80% of the implant remained 24 weeks after implantation; however, up to 72 weeks after implantation, most of the implanted HHA was resorbed. The implanted SHA was unresorbed throughout the experimental period, but degradation by the invasion of newly formed bone was seen at 72 weeks after implantation. Bone histomorphometry showed that the volume of newly formed bone and the number of osteoclasts in the implanted region were significantly higher in HHA than in SHA 24 weeks after implantation. In vitro culture of C2C12 cells with the induction of osteoblastic phenotypes using recombinant bone morphogenetic protein-2 showed similar cell density and the induction of alkaline phosphatase activity between the cells on HHA and SHA discs. In vitro osteoclastogenesis of HHA and SHA discs using bone marrow macrophages and recombinant receptor activator of nuclear factor-κB ligand showed higher TRAP activity of osteoclasts cultured on HHA discs. These results showed that slow biodegradability did not always correlate to final replaceability in bone tissue, and suggested that the activity of osteoclasts correlated to the bone-forming activity of osteoblasts.

1. Introduction

Recently, several biodegradable ceramics were developed and utilized for bone substitutes. One of the most widely-used biodegradable ceramics for bone substitutes is beta-tricalcium phosphate (β-TCP). The molar ratio of Ca/P in β-TCP is lower than that of stoichiometric hydroxyapatite. Bone substitutes made with β-TCP show biodegradability by osteoclastic resorption and more dissolubility of β-TCP in acidic solution in comparison with stoichiometric HA may partly explain the biodegradability by osteoclastic resorption [1]. However, different crystal structures between β-TCP and HA, remaining strain after material preparation and other factors may also associate with biodegradability by osteoclastic resorption.

Recently, we compared the biological natures of β-TCP composed of rod-shaped particles, which was synthesized by a unique hydrothermal method [2,3], and conventional β-TCP composed of globular-shaped particles, which was synthesized by the normal sintering method. In an in vitro study using the osteoclastogenesis system, conventional β-TCP composed of globular-shaped particles revealed excess osteoclastic resorption compared to β-TCP composed of rod-shaped particles. Implantation in rabbit femurs showed that β-TCP composed of rod-shaped particles stably maintained the total volume of bone and bone substitute, and replacement of the bone substitutes by newly formed bone was adequate. In contrast, conventional β-TCP composed of globular-shaped particles decreased the total volume of bone and bone substitute at 24 weeks after implantation, and the microstructure

* Corresponding author. Tel./fax: +81 95 819 7644.
E-mail address: tohrupth@nagasaki-u.ac.jp (T. Ikeda).
[1] Present address: Department of Crystalline Materials Science, Graduate School of Engineering, Nagoya University, Furo-cyo, Chikusa-ku, Nagoya 464-8603, Japan.

0142-9612/$ – see front matter © 2008 Elsevier Ltd. All rights reserved.
doi:10.1016/j.biomaterials.2008.03.028

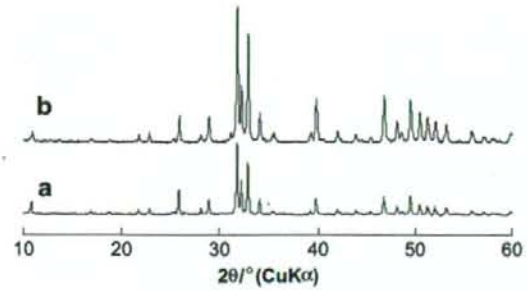

Fig. 1. X-ray diffractometry (XRD) of the implant materials used in this study. XRD patterns of HHA ceramic (a) and SHA ceramic (b).

of β-TCP was suggested to affect the biodegradability of bone substitute and metabolism of the subsequently formed bone tissue [4].

Hydroxyapatite (HA) is a major inorganic component of bone and teeth, and has long been applied for many kinds of biomaterials, including bone substitute. HA is an acid-degradable material, but stoichiometric hydroxyapatite is basically non-biodegradable when used as a bone substitute [5,6]. The molar ratio of Ca/P of hydroxyapatite in the bone was reported to be lower than the stoichiometric Ca/P ratio, 1.67 [7–9]. Osteoclastic bone resorption occurs in conjunction with acidity and proteases supplied from the ruffled border of active osteoclasts. The reason why stoichiometric HA is non-biodegradable is a very important question in the field of biomaterial science, but the answer is not clear. It is very difficult to synthesize pure calcium-deficient HA, and difficulty in comparing the biodegradability to that of pure stoichiometric HA (SHA) is one reason why we are unable to answer the question.

Previously, Ioku et al. applied a hydrothermal method to synthesize not only β-TCP described above, but also HA [10,11]. In the hydrothermal method, HA was synthesized from α-tricalcium phosphate powder, and suitable conditions enabled the synthesis of HA composed of hexagonal monocrystals with a prolonged *c*-axis. Hydrothermally synthesized HA with prolonged *c*-axis hexagonal crystals revealed rod-shaped particles by scanning electron microscopic analysis, and X-ray diffractometry (XRD) indicated that the material was uniform calcium-deficient HA [12,13]. Using hydrothermally synthesized HA composed of rod-shaped particles (HHA), it may be possible to clarify the influence of calcium deficiency and microstructure of HA on bioreactivity. In this study, we implanted HHA and SHA in rabbit femurs and histologically analyzed the biological responses. Additionally, the affinity and differentiation of bone cells on the surface of HHA and SHA were analyzed using in vitro culture systems.

2. Materials and methods

2.1. Preparation of ceramics

Cylindrical implants of HHA, 6 mm in diameter and 10 mm in length, were prepared using an applied hydrothermal method described previously [14]. The α-tricalcium phosphate (α-TCP) powder was formed into a cylindrical shape by uniaxial compressing. The formed sample was set in a 105 cm^3 autoclave with 10 cm^3 of pure water and exposed to solution vapor at 200 °C under saturated vapor pressure for 5 h. SHA implants of the same shape and size were prepared from stoichiometric HA powder with a Ca/P molar ratio of 1.67 by normal sintering at 1100 °C in air. For each implant, holes of 350 μm in diameter were created vertically and horizontally.

Discs for in vitro analyses were made as follows. For HHA discs, a slurry of α-TCP with polyvinyl alcohol was prepared at room temperature. To remove bubbles, the slurry was kept under a vacuum. Discs of α-TCP with polyvinyl alcohol were prepared from this slurry by the spin coating technique. A glass plate was set on the turntable, and then the slurry was cast on the glass plate and rotated. Discs of α-TCP with polyvinyl alcohol were dried at room temperature for about 12 h. The dried discs were cut into circles of about 12 mm in diameter, and then heated at 1200 °C for 5 min in air to remove organic matter and to keep the crystal phase of α-TCP. The samples were set in autoclave and treated hydrothermally at 180 °C for 10 h under saturated vapor pressure. SHA discs of the same shape and size were prepared from stoichiometric HA powder by normal sintering at 1100 °C in air.

2.2. Animals and operative procedures

Thirty-six female Japanese White rabbits, 3 months of age, weighing from 2.3 to 2.4 kg, were used for this study. Animals rearing and experiments were performed at the Biomedical Research Center, Center for Frontier Life Sciences, Nagasaki University, following the Guidelines for Animal Experimentation of Nagasaki University (Approval No. 0502020400/0703010564). The rabbits were anesthetized with an intramuscular injection of ketamine (60 mg/kg body weight) and xylazine (3 mg/kg body weight) before surgery. To prevent infection, a subcutaneous injection of orbifloxacin (3 mg/kg body weight) was used just before surgery. Under sterile conditions, the distal metaphysis and lateral condyle of the left femur were exposed through a 3-cm long lateral longitudinal skin incision and the thigh muscles were divided. A dead-end defect, 6 mm in diameter and 10 mm in depth, was created in the lateral cortex just proximal to the epiphyseal plate using a surgical drill. The orientation of the defect was perpendicular to the sagittal axis of the femur. The hole was irrigated with saline (0.9%), each test implant was carefully inserted into the hole manually, and the wound was closed layer by layer. Four experimental animals used for each of the HHA and SHA implants were sacrificed by an overdose of anesthetic at 2, 4, 12 and 24 weeks after the operation, and two experimental animals for each implant were sacrificed by the same method at 72 weeks after the operation. For fluorescent labeling of the bone tissue, calcein (Wako Pure Chemical Industries, Osaka, Japan) was subcutaneously injected (20 mg/kg body weight) 7 days and 1 day before sacrifice at 2 weeks after the operation, 7 days and 2 days before sacrifice at 4 weeks after the operation, and 10 days and 3 days before sacrifice at 12, 24 and 72 weeks after the operation.

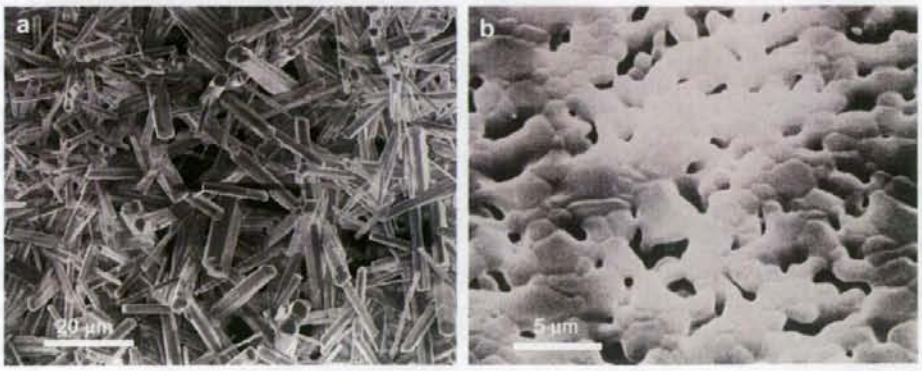

Fig. 2. Scanning electron micrographs of the microstructure of HHA and SHA.

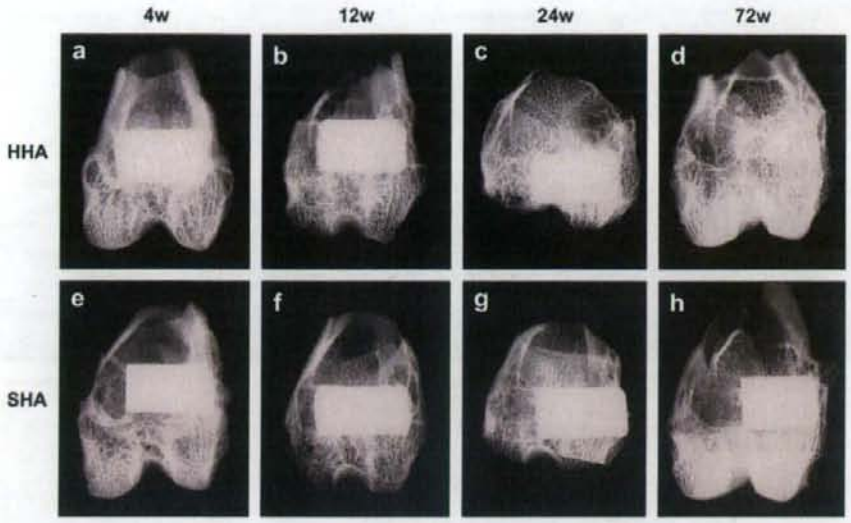

Fig. 3. Soft X-ray photographs of the operated portion of the rabbit femur. Four weeks (a), 12 weeks (b), 24 weeks (c) and 72 weeks (d) after implantation of HHA. 4 weeks (e), 12 weeks (f), 24 weeks (g) and 72 weeks (h) after implantation of SHA. Involvement of HHA in bone tissue was evident at 72 weeks (h).

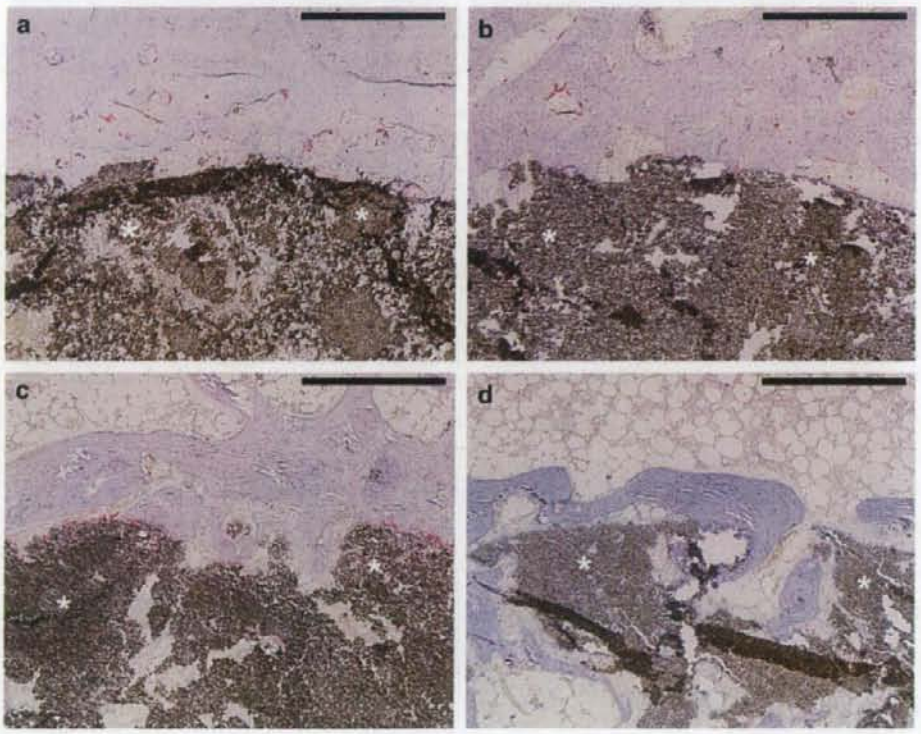

Fig. 4. Histological appearance of specimens implanted with HHA. Two weeks (a), 4 weeks (b), 12 weeks (c), and 24 weeks (d) after the operation. Sections were stained for TRAP activity. Asterisks (*) represent the implanted bone substitute. Bar: (a)–(d) 500 μm.

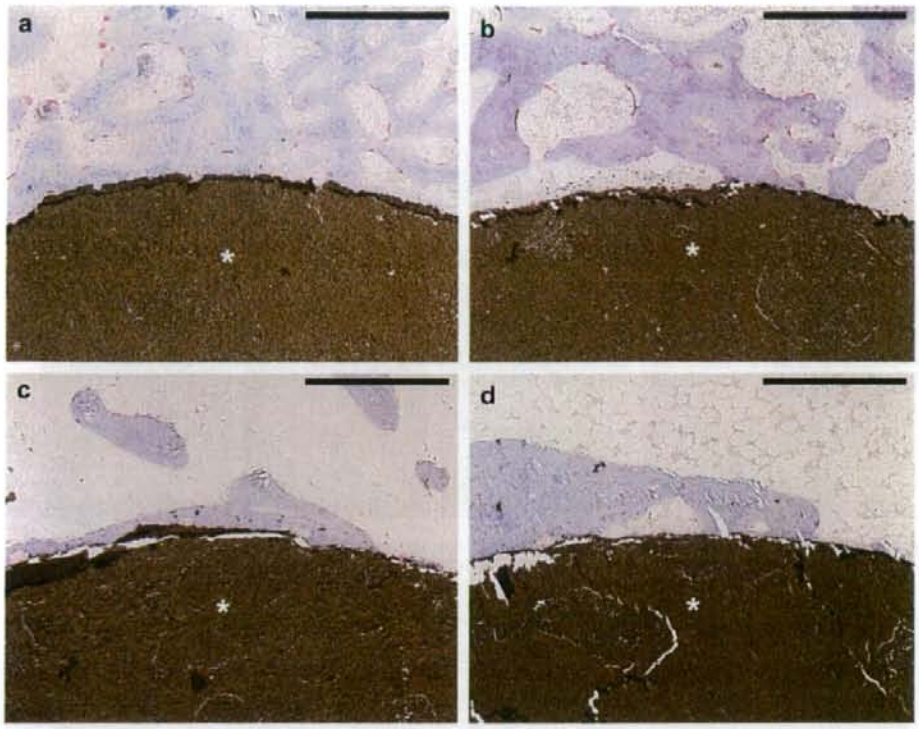

Fig. 5. Histological appearance of specimens implanted with SHA. Two weeks (a), 4 weeks (b), 12 weeks (c), and 24 weeks (d) after the operation. Sections were stained for TRAP activity. Asterisks (*) represent the implanted bone substitute. Bar: (a)–(d) 500 μm.

2.3. Radiological and histological analyses

The distal portion of the left femur was dissected from the sacrificed animals, and X-ray photographs were taken using a soft X-ray apparatus (TRS-1005, SOFRON, Tokyo, Japan). All the harvested tissue specimens were fixed in 4% formaldehyde in 0.1 M phosphate buffer (pH 7.2), embedded in 2-hydroxyethyl methacrylate/methyl methacrylate/2-hydroxyethyl acrylate mixed resin, and sectioned 3 μm thick [4]. These sections were stained with toluidine blue or histochemically stained for tartrate-resistant acid phosphatase (TRAP) activity as described previously [15].

2.4. Histomorphometry

Histomorphometric analyses were performed using the Osteoplan II system (Carl Zeiss, Thornwood, NY) as described previously [16]. Bone volume/tissue volume (BV/TV, %), bone formation rate/bone surface (BFR/BS, $mcm^3/mcm^2/d$), mineral apposition rate (MAR, mcm/d), number of osteoclasts/bone perimeter (N.Oc/B.Pm, per 100 mm), and osteoclast surface/bone surface (Oc.S/BS, %) were calculated for each sample in four squares (0.4 mm × 1.2 mm), each of which was arranged adjacent to two squares with shorter sides of 1.2 mm long, which inscribed proximodistally and antero-posteriorly in a circle of the implant 6 mm in diameter. An

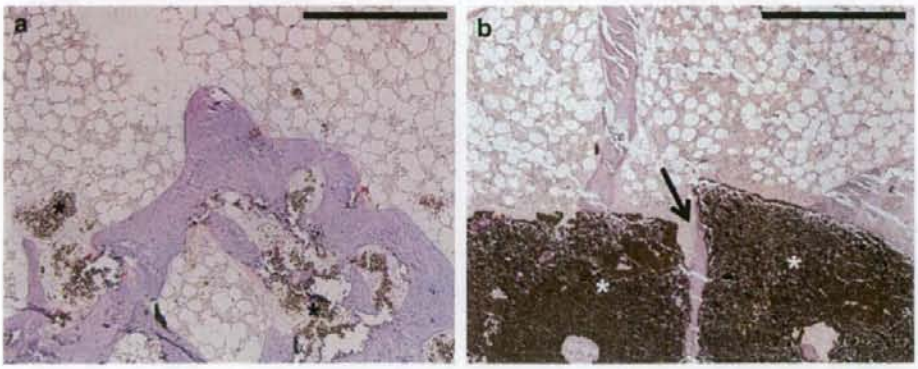

Fig. 6. Comparison of histological appearance of specimens 72 weeks after implantation of HHA and SHA. Implantation of HHA (a) and SHA (b). Sections were stained for TRAP activity. A crack in SHA with newly formed bone tissue (an arrow) was evident (b). Asterisks (*) represent the implanted bone substitute. Bar: (a) and (b) 500 μm.

osteoclast was defined as a multinucleated cell in contact with the surface of a bone or bone substitute. MAR was calculated under a fluorescence microscope at a wavelength of 455 nm. To calculate BV/TV, N.Oc/B.Pm, Oc.S/BS, and BFR/BS, sections stained with toluidine blue were used. Statistical differences were evaluated using the *t*-test.

2.5. In vitro experiments

Osteoblasts were generated using C2C12 preosteoblastic cells with stimulation of recombinant human bone morphogenetic protein-2 (Pepro Tech Inc., Rocky Hill, NJ) at a concentration of 300 ng/ml in α-minimal essential medium supplemented with 10% fetal bovine serum. The procedure followed previous reports [17]. The discs used for the experiment were fixed with methanol/acetone (6:4) fixative, and stained for alkaline phosphatase (ALP) activity on the 6th day of culture.

Osteoclasts were generated using mouse bone marrow macrophages prepared from the femora and tibiae of 5-week-old female ddY mice and recombinant soluble isoform of mouse receptor activator of nuclear factor-κB ligand (RANKL) [15,18]. Bone marrow macrophages (4×10^4 cells/well) were seeded in 48-well plates in which an HHA or SHA disc, 8 mm in diameter, was inserted per well and maintained with culture medium supplemented with 10% fetal calf serum, 30 ng/ml of mouse macrophage colony stimulating factor (M-CSF) (Sigma, St. Louis, MO) and 200 ng/ml of recombinant mouse RANKL synthesized using GST system (Amersham Pharmacia Biotech Inc., Piscataway, NJ) as reported previously [18]. All ceramic discs were presoaked in α-minimal essential medium supplemented with 10% fetal calf serum for 4 weeks, changing the culture medium every week before being used for experiments. The medium of the cultures was changed every other day. The discs used for the experiment were fixed with methanol/acetone (6:4) fixative, and stained for TRAP activity on the 8th day of culture. To analyze the viability of the cultures, the discs used for the experiment were fixed with the same fixative described above and stained the nuclei with DAPI (Dojindo Laboratories, Kumamoto, Japan). The stained nuclei were viewed under a fluorescence microscope at a wavelength of 455 nm.

3. Results

3.1. General features of samples

Synthesized HHA and SHA were analyzed by powder X-ray diffractometry with graphite-monochromatized CuKα radiation, operating at 40 kV and 20 mA (XRD; Multi Flex, Rigaku, Tokyo, Japan). No phase other than HA was detected for HHA, which was hydrothermally synthesized at 200 °C for 5 h and SHA, which was synthesized by sintering at 1100 °C (Fig. 1a,b). These results showed that both HHA and SHA were pure and uniform HA. When HHA was sintered at 900 °C, decomposition of HA to β-TCP was detected because the HHA was nonstoichiometric HA of calcium-deficient composition. There was no decomposition as a result of sintering in the case of SHA because SHA was stoichiometric (data not shown). The results corresponded to chemical analysis by ICP-MS (Seiko Inst., SPQ9000S, Japan). The surface of HHA and SHA was analyzed by scanning electron microscope (JSM-T300, JEOL, Tokyo, Japan). Pore volume and distribution of pore diameter were measured by mercury intrusion porosimetry (MIP; Carlo Elba, Porosimeter 2000, Italy). HHA was composed of rod-shaped particles about 20 μm in length, which were tangled together to form micropores about 0.2 μm in size (Fig. 2a). SHA was composed of globular particles, which fused to one another and formed micropores about 0.5 μm in size (Fig. 2b). The porosity of HHA and SHA was 70%.

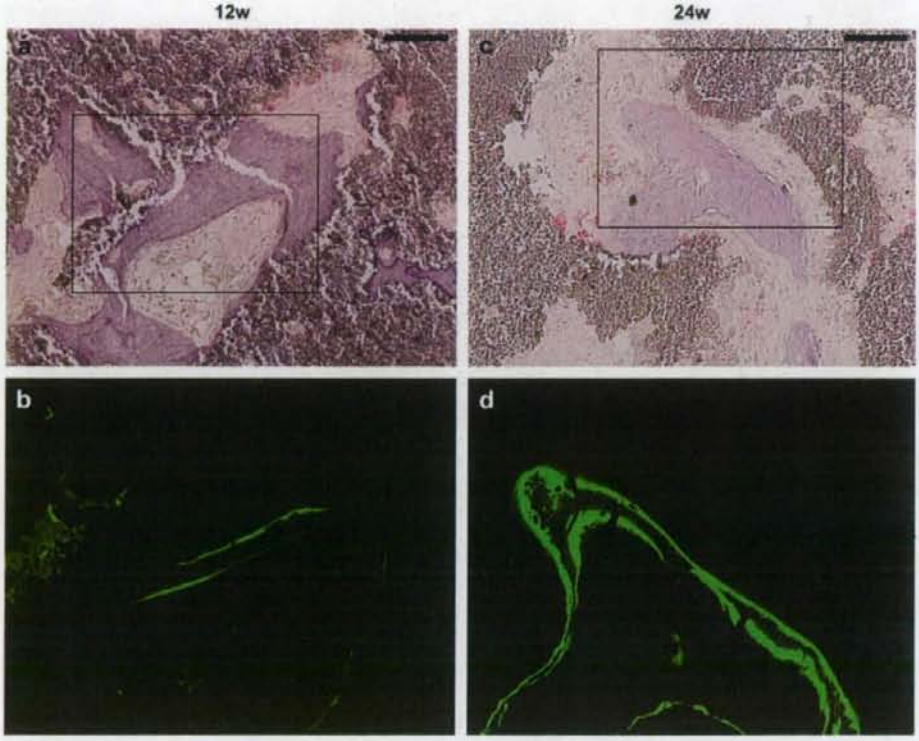

Fig. 7. Evaluation of osteogenesis in a specimen implanted with HHA by fluorescent labeling. (a,c) Bright-field light microscopic appearance of specimens 12 weeks (a) and 24 weeks (c) after HHA implantation. Sections were stained for TRAP activity. The rectangles represent the area used for fluorescent analysis. (b,d) The calcein signal in newly formed bone tissue in the specimens 12 weeks (b) and 24 weeks (d) after HHA implantation. Sections stained with toluidine blue were utilized for analysis by fluorescence microscopy. Bar: (a,c) 100 μm.